

---

# A NEW FAMILY OF DUAL-NORM REGULARIZED $p$ -WASSERSTEIN METRICS

---

A PREPRINT

**Piyushi Manupriya**  
IIT Hyderabad, India

**J. Saketha Nath**  
IIT Hyderabad, India

**Pratik Jawanpuria**  
Microsoft IDC, India

November 8, 2022

## ABSTRACT

We develop a novel family of metrics over measures, using  $p$ -Wasserstein style optimal transport (OT) formulation with dual-norm based regularized marginal constraints. Our study is motivated by the observation that existing works have only explored  $\phi$ -divergence regularized Wasserstein metrics like the Generalized Wasserstein metrics or the Gaussian-Hellinger-Kantorovich metrics. It is an open question if Wasserstein style metrics can be defined using regularizers that are not  $\phi$ -divergence based. Our work provides an affirmative answer by proving that the proposed formulation, under mild conditions, indeed induces valid metrics for any dual norm. The proposed regularized metrics seem to achieve the best of both worlds by inheriting useful properties from the parent metrics, viz., the  $p$ -Wasserstein and the dual-norm involved. For example, when the dual norm is Maximum Mean Discrepancy (MMD), we prove that the proposed regularized metrics inherit the dimension-free sample complexity from the MMD regularizer; while preserving/enhancing other useful properties of the  $p$ -Wasserstein metric. Further, when  $p = 1$ , we derive a Fenchel dual, which enables proving that the proposed metrics actually induce novel norms over measures. Also, in this case, we show that the mixture geodesic, which is a common geodesic for the parent metrics, remains a geodesic. We empirically study various properties of the proposed metrics and show their utility in diverse applications.

## 1 Introduction

Optimal transport (OT) has witnessed a lot of success in machine learning applications [49]. OT's success is partly due to clever regularization [17], which plays a critical role in handling noisy marginals [24] or marginals of unequal masses [12, 37], and in affecting the computational complexity [4, 3] as well as the sample complexity [43, 39, 26, 23].

Optimal transport with Kullback Leibler (KL), and in general,  $\phi$ -divergence, based regularization is a very well-understood topic [36, 37, 11, 13, 12]. Regularizers based on Total Variation (TV) are also well-studied [50, 51, 29, 27]. In particular, the Generalized Wasserstein (GW) metrics and the Gaussian-Hellinger-Kantorovich (GHK) metrics are defined using TV and KL based regularizations, respectively. The above works also study some interesting properties of the GW and GHK metrics.

On the other hand, it seems regularization apart from the  $\phi$ -divergence is rather unexplored in the context of optimal transport. The only exception seems to be [43], which showed that Maximum Mean Discrepancy (MMD) [42] based regularization for OT, unlike the popular KL based regularization, leads to a completely dimension-free bound on the sample complexity of estimation. However, it is an open question if valid metrics could be defined using the sample-efficient MMD based regularization.

In this work we not only provide an affirmative answer to this open question, but also study OT regularization based on a generic family of dual norms, also known as Integral Probability Metrics (IPMs) [56]. IPMs are metrics induced by dual norms over measures and include MMD as a special case. Also, they are a family of metrics complementary to the  $\phi$ -divergences, with the TV metric being the only common member. To the best of our knowledge, our work is the first to study IPM regularization in the context of OT.

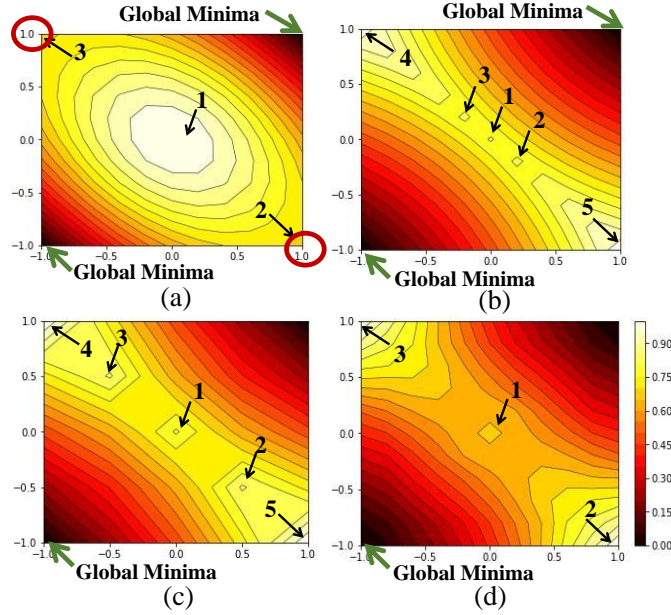


Figure 1: Level sets of distance function between a family of source distributions and a fixed target distribution with the task of finding the source distribution closest to the target distribution using (a) MMD, (b) OT with no regularization, (c) OT with TV regularization, and (d) OT with proposed MMD regularization. While global minima (marked with Green arrows) is correctly identified by all methods, level sets with the proposed MMD-regularized OT show no local minima (encircled in Red for MMD) and have lesser number of non-optimal stationary points (marked with Black arrows) compared to (b) and (c). Please refer to Section 4.1 details.

We begin by introducing a novel family of  $p$ -Wasserstein style OT formulations that employ IPM-regularization for matching the marginals. We focus on  $p = 1$  and  $p > 1$  settings. In the first setting ( $p = 1$ ) we prove that the proposed formulation induces a valid metric over measures for any IPM. By deriving a Fenchel dual, we show that the metrics can be understood as a  $q$ -degree infimal convolution of the 1-Wasserstein metric and the IPM employed for regularization. From this, it follows that the proposed metrics in this setting are in fact norm-induced ones. Further, in the special case  $p = 1, q = 1$ , we show that these metrics, in fact, belong to the IPM family itself. However, when  $p = 1, q > 1$ , the proposed metrics are new and, as far as we know, do not belong to any previously studied class of metrics. In the second setting ( $p > 1$ ), we prove that the proposed IPM-regularized  $p$ -Wasserstein formulation induces a pre-metric satisfying the sub-additive property.

Interestingly, the proposed regularized metrics seem to be inheriting the desirable properties from the parent metrics (the  $p$ -Wasserstein and the IPM involved) while avoiding their inherent limitations. For example, in the special case the IPM is MMD, we prove that the sample complexity is inherited from the MMD metric, whose sample complexity is dimension-free, and not from the Wasserstein metric, whose sample complexity is plagued with the curse of dimensionality [47]. Interestingly, other interesting properties of the  $p$ -Wasserstein metric seem to be inherited: following the synthetic setup of [9], we observe in Figure 1 that the proposed metric is better suited for generative modeling than the MMD. Also, it seems to inherit the loss surface mainly from the Wasserstein metric rather than from the MMD metric. More such comparisons are detailed in section 4. For this special case, we present a finite sample-based simplified formulation for estimating the metric. We also present a formulation for solving the corresponding barycenter problem. We show that these sample-based formulations turn out to be instances of smooth convex quadratic programs, and hence propose to solve them using the accelerated projected gradient descent method [45, 6].

We report the performance of our MMD-regularized Wasserstein metric on applications such as two-sample hypothesis testing, domain adaptation, and class-ratio estimation using benchmark datasets. The results illustrate the efficacy of our methodology compared to existing OT variants. Our results on single-cell RNA sequencing further validate the quality of barycenter interpolation obtained by our approach.

## 2 Preliminaries

**Notations.** Let  $\mathcal{X}$  be a set (domain) that forms a compact Hausdorff space. Let  $\mathcal{R}^+(\mathcal{X})$ ,  $\mathcal{R}(\mathcal{X})$  denote the set of all non-negative, signed (finite) Radon measures defined over  $\mathcal{X}$ ; while the set of all probability measures is denoted by  $\mathcal{P}(\mathcal{X})$ . For a measure on the product space,  $\pi \in \mathcal{R}^+(\mathcal{X} \times \mathcal{X})$ , let  $\pi_1, \pi_2$  denote the first and second marginals, respectively (i.e., they are the push-forwards under the canonical projection maps onto  $\mathcal{X}$ ). Let  $\mathcal{L}(\mathcal{X})$ ,  $\mathcal{C}(\mathcal{X})$  denote the set of all real-valued measurable functions and all real-valued continuous functions, respectively, over  $\mathcal{X}$ .

### 2.1 Integral Probability Metrics a.k.a. Dual Norms

Given a set  $\mathcal{G} \subset \mathcal{L}(\mathcal{X})$ , the Integral Probability Metric (IPM) [42, 56, 1], or the dual norm, associated with  $\mathcal{G}$ , is defined by:

$$\gamma_{\mathcal{G}}(s_0, t_0) \equiv \max_{f \in \mathcal{G}} \left| \int_{\mathcal{X}} f \, ds_0 - \int_{\mathcal{X}} f \, dt_0 \right| \quad \forall s_0, t_0 \in \mathcal{R}^+(\mathcal{X}). \quad (1)$$

Classical examples of IPMs include:

**Kantorovich:** Let  $d$  be a given (ground) metric over the domain  $\mathcal{X} \times \mathcal{X}$ . Let,  $\|f\|_d \equiv \max_{x \in \mathcal{X} \neq y \in \mathcal{X}} \frac{|f(x) - f(y)|}{d(x, y)}$ , denote the Lipschitz constant of  $f$  with respect to the metric  $d$ . Kantorovich metric is the IPM associated with the generating set:  $\mathcal{W}_d \equiv \{f : \mathcal{X} \mapsto \mathbb{R} \mid \|f\|_d \leq 1\}$ . From the Kantorovich-Fenchel duality we have that the Kantorovich metric, when restricted to the set of probability measures,  $\mathcal{P}(\mathcal{X})$ , is same as the **1-Wasserstein** metric.

**Maximum Mean Discrepancy (MMD):** Let  $k$  be a characteristic kernel [57] over the domain  $\mathcal{X}$ . Let  $\|f\|_k$  denote the norm of  $f$  in the canonical reproducing kernel Hilbert space (RKHS),  $\mathcal{H}_k$ , corresponding to  $k$ . MMD is the IPM associated with the generating set:  $\mathcal{M}_k \equiv \{f \in \mathcal{H}_k \mid \|f\|_k \leq 1\}$ .

**Total Variation (TV):** This is the IPM associated with the generating set:  $\mathcal{T} \equiv \{f : \mathcal{X} \mapsto \mathbb{R} \mid \|f\|_{\infty} \leq 1\}$ , where  $\|f\|_{\infty} \equiv \max_{x \in \mathcal{X}} |f(x)|$ .

**Dudley:** This is the IPM associated with the generating set:  $\mathcal{D}_d \equiv \{f : \mathcal{X} \mapsto \mathbb{R} \mid \|f\|_{\infty} + \|f\|_d \leq 1\}$ , where  $d$  is a ground metric over  $\mathcal{X} \times \mathcal{X}$ . The so-called **Flat** metric is related to the Dudley metric. Its generating set is:  $\mathcal{F}_d \equiv \{f : \mathcal{X} \mapsto \mathbb{R} \mid \|f\|_{\infty} \leq 1, \|f\|_d \leq 1\}$ .

**Kolmogorov:** Let  $\mathcal{X} = \mathbb{R}^n$ . Then, Kolmogorov metric is the IPM associated with the generating set:  $\mathcal{K} \equiv \{1_{(-\infty, x)} \mid x \in \mathbb{R}^n\}$ .

In order that the IPM metrizes weak convergence, we assume the following [42]:

**Assumption 2.1.**  $\mathcal{G}$  is dense in  $\mathcal{C}(\mathcal{X})$  and is compact.

Since the IPM generated by  $\mathcal{G}$  and its absolute convex hull are the same, (without loss of generality) we additionally assume the following:

**Assumption 2.2.**  $\mathcal{G}$  is absolutely convex.

### 2.2 Optimal Transport

Given a cost function,  $c : \mathcal{X} \times \mathcal{X} \mapsto \mathbb{R}$ , and two probability measures  $s_0 \in \mathcal{P}(\mathcal{X})$ ,  $t_0 \in \mathcal{P}(\mathcal{X})$ , the  $p$ -Wasserstein Kantorovich OT formulation is given by:

$$\bar{W}_p^p(s_0, t_0) \equiv \min_{\pi \in \mathcal{P}(\mathcal{X} \times \mathcal{X})} \int c^p \, d\pi, \text{ s.t. } \pi_1 = s_0, \pi_2 = t_0. \quad (2)$$

An optimal solution of (2) is called as a transport plan. Whenever the cost is a metric,  $d$ , over  $\mathcal{X}$  (ground metric),  $\bar{W}_p$  defines another metric, known as the  $p$ -Wasserstein metric, over  $\mathcal{P}(\mathcal{X}) \times \mathcal{P}(\mathcal{X})$ . This has many applications: as a loss function [24], for measure interpolation [28], etc. The Kantorovich-Fenchel duality result shows that the 1-Wasserstein metric is same as the Kantorovich metric, when restricted to probability measures.

In case the given measures,  $s_0, t_0 \in \mathcal{P}(\mathcal{X})$ , it may happen that they are of unequal masses. This is known as the unbalanced optimal transport (UOT) setting. In UOT or when the measures are uncertain (perhaps sample based), one employs a regularized version [37, 11]:

$$\min_{\pi \in \mathcal{P}(\mathcal{X} \times \mathcal{X})} \int c \, d\pi + \lambda D_{\phi}(\pi_1, s_0) + \lambda D_{\phi}(\pi_2, t_0), \quad (3)$$

where  $D_\phi$  is the divergence generated by  $\phi$ . In the special case  $D_\phi$  is the KL divergence and the ground cost  $c$  is squared-Euclidean, the optimal objective of (3) is square of the so-called Gaussian Hellinger-Kantorovich metric [37] between the marginals  $s_0, t_0$ .

[51] studied a Total Variation metric (denoted by  $|\cdot|_{TV}$ ) regularized OT formulation:

$$\min_{\pi \in \mathcal{R}^+(\mathcal{X} \times \mathcal{X})} |\pi|^{p-1} \int c^p d\pi + \lambda |\pi_1 - s_0|_{TV}^p + \lambda |\pi_2 - t_0|_{TV}^p, \quad (4)$$

where  $|\pi|$  is the mass of measure  $\pi$ . The  $p^{th}$ -root of the optimal objective of (4) is the so-called Generalized Wasserstein metric between  $s_0, t_0$ .

### 3 Proposed IPM-regularized OT

In this section, we study the proposed IPM-regularized OT formulations. The proofs of all the results are provided in the Appendices. To begin with, consider the following novel family of OT formulations:

$$(\mathcal{U}_{\mathcal{G},c,\lambda,p,q}(s_0, t_0))^q \equiv \min_{\pi \in \mathcal{R}^+(\mathcal{X} \times \mathcal{X})} \left( |\pi|^{p-1} \int c^p d\pi \right)^{q/p} + \lambda \gamma_{\mathcal{G}}^q(\pi_1, s_0) + \lambda \gamma_{\mathcal{G}}^q(\pi_2, t_0), \quad (5)$$

where  $\gamma_{\mathcal{G}}$  is the IPM associated with the generating set,  $\mathcal{G}$ ,  $\lambda > 0$  is the regularization hyperparameter,  $|\pi|$  denotes the mass of measure  $\pi$ , and  $p \geq 1, q \geq 1$ .

**Lemma 3.1.** *The above can be equivalently re-written in the following form:*

$$(\mathcal{U}_{\mathcal{G},c,\lambda,p,q}(s_0, t_0))^q = \min_{s,t \in \mathcal{R}^+(\mathcal{X})} |s|^q (W_p(s, t))^q + \lambda \gamma_{\mathcal{G}}^q(s, s_0) + \lambda \gamma_{\mathcal{G}}^q(t, t_0), \quad (6)$$

$$\text{where } W_p(s, t) \equiv \begin{cases} \bar{W}_p\left(\frac{s}{|s|}, \frac{t}{|t|}\right) & \text{if } |s| = |t|, \\ \infty & \text{otherwise.} \end{cases}$$

We give proof of the above lemma in appendix Section A. In the special case  $p = q$  or  $q = 1$ , and  $\mathcal{G}$  is the unit  $\infty$ -norm ball,  $\mathcal{U}$  recovers the Generalized Wasserstein metric, (4). As far as we know, it is an open question if  $\mathcal{U}$  is a metric for arbitrary generating sets and in particular, the sample-efficient MMD metric. We fill this gap in literature by analyzing metric properties of (5) and (6) with a general  $\mathcal{G}$  in two special cases: the case of  $p = 1$  is presented in Section 3.1 and that of  $p > 1$  is presented in Section 3.2.

#### 3.1 Case: $p = 1$

The metric property in this case is given by the following theorem:

**Theorem 3.2.** *Let  $\mathcal{G}$  satisfy Assumption 2.1, then  $\gamma_{\mathcal{G}}$  is a valid IPM. Let  $c$  be a ground metric over  $\mathcal{X} \times \mathcal{X}$  and  $\lambda > 0, q > 1$ . Then,  $\mathcal{U}_{\mathcal{G},c,\lambda,1,q}$  induces a novel interpolation norm [14] between the Kantorovich norm and the dual norm used for regularization.*

We give proof of the above theorem in appendix Section B.

**Remark 3.3.** *In general, when the IPM is not the TV metric, and  $q > 1$ , the proposed metrics  $\mathcal{U}_{\mathcal{G},c,\lambda,1,q}$  do not belong to any known class of metrics over measures.*

In the case  $q = 1$ , as shown in the following theorem, the metrics  $\mathcal{U}_{\mathcal{G},c,\lambda,1,1}$  belong to the IPM family:

**Theorem 3.4.** *Whenever  $\mathcal{G}$  satisfies Assumptions 2.1 and 2.2,  $c$  is a (continuous) ground metric over compact  $\mathcal{X} \times \mathcal{X}$ , and  $\lambda > 0$ , we have that:*

$$\mathcal{U}_{\mathcal{G},c,\lambda,1,1}(s_0, t_0) = \max_{f \in \mathcal{G}(\lambda) \cap \mathcal{W}_c} \int_{\mathcal{X}} f ds_0 - \int_{\mathcal{X}} f dt_0. \quad (7)$$

Here,  $\mathcal{G}(\lambda) \equiv \{\lambda g \mid g \in \mathcal{G}\}$  and  $\mathcal{W}_c$  is all 1-Lipschitz functions wrt. metric  $c$ .

We give proof of the above theorem in appendix Section C.

**Remark 3.5.** *If  $\mathcal{G}$  is the unit uniform-norm ball (corresponding to TV), our result specializes to that in [51], which proves that  $\mathcal{U}$  coincides with the so-called Flat metric (or the bounded Lipschitz distance).*

**Remark 3.6.** If the regularizer is the Kantorovich metric<sup>1</sup>, i.e.,  $\mathcal{G} = \mathcal{W}_c$ , and  $\lambda \geq 1$ , then  $\mathcal{U}_{\mathcal{W}_c, c, \lambda, 1, 1}$  coincides with the Kantorovich metric. In other words, the Kantorovich-regularized OT is same as the Kantorovich metric. Thus, our proposed formulation (5) provides the OT interpretation for the Kantorovich metric, which is valid for all (potentially un-normalized) measures in  $\mathcal{R}^+(\mathcal{X})$ .

The proofs of theorems 3.2 & 3.4 are based on deriving a Fenchel dual. Theorem 3.2 not only implies that the proposed metrics are norm-induced, but are in fact a particular interpolation between the parent norms. Hence, they are expected to inherit/improve properties of their parent norms (see section 3.3 for more details). As discussed in [14], interpolation norms over  $\mathbb{R}^n$  are popularly employed in function induction as sophisticated regularizers and the corresponding optimization problems can be solved efficiently.

### 3.2 Case: $p > 1$

In this case, metric properties like non-negativity, positive-definiteness, and symmetry trivially are inherited by  $\mathcal{U}_{\mathcal{G}, c, \lambda, p, p}$ . We also prove that  $\mathcal{U}_{\mathcal{G}, c, \lambda, p, p}^p$  is convex:

**Theorem 3.7.** For any  $\mathcal{G}, c, \lambda \geq 0, p > 1$ ,  $\mathcal{U}_{\mathcal{G}, c, \lambda, p, p}^p$ , defined in (5), is a convex function over  $\mathcal{R}_1^+(\mathcal{X}) \times \mathcal{R}_1^+(\mathcal{X})$ .

Recall that  $p$ -Wasserstein metric may not be convex when  $p > 1$ , but,  $W_p^p$  is convex (Theorem 4.8 in [63]). Thus, theorem 3.7 proves that this useful property of  $W_p^p$  is inherited by the proposed  $\mathcal{U}_{\mathcal{G}, c, \lambda, p, p}^p$ .

We give proof of the above theorem in appendix Section D.

### 3.3 Additional Properties

In this section we analyze the proposed formulation and induced metrics/norms. Some of the properties are inherited/improved from the parent metrics, while others are due to the form of the regularized formulation.

**Sample Complexity.** Unlike existing classes of regularized OT metrics, the key advantage is that our metrics include the sample-efficient MMD regularization. A close observation of [43]’s proof strategy shows that the MMD regularized OT inherits its dimension-free sample complexity from that of MMD. Generalizing this result, we present the following theorem:

**Theorem 3.8.** Let  $\lambda > 0, p \geq 1, q \geq 1$ . Let us denote  $\mathcal{U}_{\mathcal{G}, c, \lambda, p, q}$ , defined in (5), by  $\bar{\mathcal{U}}_q$ . Let  $\hat{s}_m, \hat{t}_m$  denote the empirical estimates of  $s_0, t_0$  respectively with  $m$  samples. Then,  $\bar{\mathcal{U}}_1(\hat{s}_m, \hat{t}_m) \rightarrow \bar{\mathcal{U}}_1(s_0, t_0)$  at a rate same as that of  $\gamma_{\mathcal{G}}(\hat{s}_m, s_0) \rightarrow 0$ . Further,  $\bar{\mathcal{U}}_q^q(\hat{s}_m, \hat{t}_m) \rightarrow \bar{\mathcal{U}}_q^q(s_0, t_0)$  at a rate same as that of  $\gamma_{\mathcal{G}}(\hat{s}_m, s_0) \rightarrow 0$ .

We give proof of the above theorem in appendix Section E.1. In particular, when the IPM is the MMD, the proposed metrics enjoy dimension-free sample complexity.

**Geodesic analysis.** The geometry induced by a metric is often understood from its geodesics. To this end, we present the following lemma:

**Lemma 3.9.** For any two measures  $s_0, s_1 \in \mathcal{R}^+(\mathcal{X})$ , the mixture measures  $\forall t \in [0, 1], s_t = (1 - t)s_0 + ts_1$  form a curve in the space of measures  $\mathcal{R}^+(\mathcal{X})$ . Any mixture curve joining two measures  $s_0, s_1 \in \mathcal{R}^+(\mathcal{X})$  such that  $\mathcal{U}_{\mathcal{G}, c, \lambda, 1, q}(s_0, s_1) < \infty$ , is a constant speed minimal geodesic, making  $\mathcal{U}_{\mathcal{G}, c, \lambda, 1, q}$  a strictly intrinsic distance.

We give more details on geodesic in appendix Section E.2 and the proof of the above lemma in E.5. While the mixture geodesic is a common geodesic for all IPMs [9], the above result shows that it is inherited by the proposed metrics. Depending on the IPM employed, there may be other geodesic(s) for the proposed metric.

**Robustness analysis.** Since the marginals in (5) are matched in a soft manner, it is expected that such regularized OT formulations are robust to uncertainties/noise in the marginals. This is formalized in the lemma below:

**Lemma 3.10.** Let  $s, t \in \mathcal{R}^+(\mathcal{X})$  be two measures such that  $s$  is corrupted with  $\rho$  fraction of outliers i.e.,  $s = (1 - \rho)s_c + \rho s_o$ , where  $s_c$  is the clean measure and  $s_o$  is the outlier measure. Let  $|s_c - s_o|_{TV} \leq \epsilon$ . Then,

$$\mathcal{U}_{\mathcal{G}, c, \lambda, 1, 1}(s, t) \leq \mathcal{U}_{\mathcal{G}, c, \lambda, 1, 1}(s_c, t) + \rho\beta\epsilon,$$

where  $\beta = \max_{f \in \mathcal{G}(\lambda) \cap \mathcal{W}_c} \|f\|_{\infty}$ .

<sup>1</sup>The ground metric in  $\mathcal{U}$  must be same as that defining the Kantorovich regularizer.

For the case  $q > 1$ ,

$$\mathcal{U}_{G,c,\lambda,1,q}(s, t) \leq \mathcal{U}_{G,c,\lambda,1,q}(s_c, t) + \frac{\eta^{1/q}}{\alpha^r} t \rho \beta \epsilon$$

where  $\frac{1}{q} + \frac{1}{r} = 1$ ,  $t = \min\left(1, \frac{\lambda^{1/q}}{2^r}\right)$ ,  $\alpha = \frac{q-1}{q^r}$ ,  $\eta = \frac{r-1}{r^q}$ .

We give proof of the above lemma in appendix Section E.3.

### 3.4 Finite Sample Simplifications

Encouraged by the above theoretical results, we now focus on few pragmatic details for employing the proposed metrics in machine learning (ML) applications. For the sake of simplicity of presentation, we consider the following MMD regularized variant in this section:

$$\mathcal{U}(s_1, s_2) \equiv \min_{\pi \in \mathcal{R}^+(\mathcal{X} \times \mathcal{X})} \int c^2 d\pi + \lambda_1 \|\mu_{\pi_1} - \mu_{s_1}\|^2 + \lambda_2 \|\mu_{\pi_2} - \mu_{s_2}\|^2, \quad (8)$$

Here,  $\mu_s \equiv \int \phi(x) ds(x)$  is the kernel mean embedding of  $s$  [41],  $\phi$  is the canonical feature map, and  $\|\cdot\|$  denotes the RKHS norm associated with a given characteristic kernel  $k$ .

In typical ML applications, only samples from  $s_i$  are available. Accordingly, the support of the optimal plan is assumed to be finite/fixed and estimation is performed. Let  $m_i$  samples from  $s_i$  be given:  $\mathcal{D}_i = \{x_{i1}, \dots, x_{im_i}\}$ . Let us denote the Gram-matrix of  $\mathcal{D}_i$  by  $G_{ii}$ . Let  $\mathcal{C}_{12}$  be the  $m_1 \times m_2$  cost matrix with entries as evaluations of function  $c^2$  over  $\mathcal{D}_1 \times \mathcal{D}_2$ . As mentioned earlier, let us assume the transport plan is supported only at the samples<sup>2</sup>: let  $\alpha_{ij} \equiv \pi(x_{1i}, x_{2j})$ . Then,  $\mu_{\pi_1} = \frac{1}{m_1} \sum_{i=1}^{m_1} \sum_{j=1}^{m_2} \alpha_{ij} \phi(x_{1i})$ ,  $\mu_{\pi_2} = \frac{1}{m_2} \sum_{j=1}^{m_2} \sum_{i=1}^{m_1} \alpha_{ij} \phi(x_{2j})$  and the estimate of  $\mu_{s_i}$  is  $\frac{1}{m_i} \sum_{j=1}^{m_i} \phi(x_{ij})$ . With this notation, (8) simplifies as:

$$\min_{\alpha \geq 0 \in \mathbb{R}^{m_1 \times m_2}} \text{Tr}(\alpha \mathcal{C}_{12}^\top) + \lambda_1 \|\alpha \mathbf{1} - \frac{\sigma_1}{m_1} \mathbf{1}\|_{G_{11}}^2 + \lambda_2 \|\alpha^\top \mathbf{1} - \frac{\sigma_2}{m_2} \mathbf{1}\|_{G_{22}}^2, \quad (9)$$

where  $\text{Tr}(M)$  denotes the trace of matrix  $M$  and  $\|x\|_M^2 \equiv x^\top M x$ .

A related problem is that of barycenter interpolation of measures [2], which has interesting applications [55, 54, 28]. Given measures  $s_1, \dots, s_n$  with total masses  $\sigma_1, \dots, \sigma_n$  respectively, and interpolation weights  $\rho_1, \dots, \rho_n$ , the barycenter  $s \in \mathcal{R}^+(X)$  is defined as the solution of

$$\min_{s \in \mathcal{R}^+(X)} \sum_{i=1}^n \rho_i \mathcal{U}(s_i, s). \quad (10)$$

In typical ML applications, only sample sets,  $\mathcal{D}_i$ , from  $s_i$  are available instead of  $s_i$  themselves. Following [18], we assume<sup>3</sup> that the barycenter,  $s$ , is supported by  $\cup_{i=1}^n \mathcal{D}_i$  and  $\beta \in \mathbb{R}^m$  denotes the corresponding probabilities. Here,  $m = \sum_{i=1}^n m_i$ . Accordingly, we assume that the transport plan  $\pi^i$  corresponding to  $\mathcal{U}(s_i, s)$  is supported by  $\mathcal{D}_i \times \cup_{i=1}^n \mathcal{D}_i$  and let  $\alpha_i \geq 0 \in \mathbb{R}^{m_i \times m}$  denote the corresponding probabilities. Let  $G$  be the Gram-matrix of  $\cup_{i=1}^n \mathcal{D}_i$ . Let  $\mathcal{C}_i$  be the  $m_i \times m$  matrix with entries as evaluations of cost function,  $c^2$ . The proposed barycenter formulation (10) simplifies as:

$$\min_{\alpha_i, \beta \geq 0} \sum_{i=1}^n \rho_i \left\{ \text{Tr}(\alpha_i \mathcal{C}_i^\top) + \lambda_1 \|\alpha_i \mathbf{1} - \frac{\sigma_i}{m_i} \mathbf{1}\|_{G_i}^2 + \lambda_2 \|\alpha_i^\top \mathbf{1} - \beta\|_G^2 \right\}. \quad (11)$$

The minimization with respect to  $\beta$  is a standard weighted least-squares problem, which gives the analytical solution:  $\beta = \sum_{j=1}^n \rho_j \alpha_j^\top \mathbf{1}$ . Using this to eliminate  $\beta$ , leads to

$$\min_{\alpha_i \geq 0} \sum_{i=1}^n \rho_i \left( \text{Tr}(\alpha_i \mathcal{C}_i^\top) + \lambda_1 \|\alpha_i \mathbf{1} - \frac{\sigma_i}{m_i} \mathbf{1}\|_{G_i}^2 + \lambda_2 \|\alpha_i^\top \mathbf{1} - \sum_{j=1}^n \rho_j \alpha_j^\top \mathbf{1}\|_G^2 \right). \quad (12)$$

<sup>2</sup>We can also assume the support is  $\mathcal{D}_1 \cup \mathcal{D}_2$  on both sides.

<sup>3</sup>Analogous derivations can be done with any other such finite parameterizations too.

Problems (9) & (12) are instances of convex quadratic programs with non-negativity constraints. In the setting where all involved measures are normalized, the non-negativity constraints can be replaced by simplex constraints.

In the following result, we show that the gradient of the objective in Problem (9) is  $L$ -smooth, which enables us to use the projected accelerated gradient decent algorithm [45, 44, 6] with fixed step-size  $\tau = 1/L$  for solving (9). Analogous result may also be derived for (12).

**Lemma 3.11.** *The gradient of the objective in Problem (9) is smooth with smoothness constant  $L = 2\lambda\sqrt{m_2^2\|G_1\|^2 + m_1^2\|G_2\|^2 + 2(\mathbf{1}^\top G_1 \mathbf{1} + \mathbf{1}^\top G_2 \mathbf{1})}$ .*

We give proof of the above lemma in appendix Section F.

## 4 Experiments

In Section 3, we examined the theoretical properties of the proposed IPM-regularized OT formulations. In this section, our aim is to show that IPM regularization for marginal constraints for OT is a viable practical alternative to the popular KL-divergence regularized marginal constraints. Though the proposed MMD regularized formulation (9) obtains good empirical results on different applications, our purpose is not to benchmark state-of-the-art performance.

**Baselines.** On synthetic datasets, we compare against the 2-Wasserstein, Generalized Wasserstein (GW-TV) [51] and MMD baselines. In noisy setting, we also show efficacy of the proposed method over robust OT methods such as ROT [5] and RSOT [33]. We compare our approach with KL-divergence regularized unbalanced OT formulation with entropy regularization [12] ( $\epsilon$ KL-UOT) and MMD metric on real-world datasets.

For GW-TV, we show qualitative results only with  $p = 1$  case (solved using Linear Programming) due to computational constraints. For OT based approaches, the ground metric is tuned between Euclidean and squared-Euclidean cost. For kernel based formulations, such as MMD and the proposed (9), we tune the characteristic kernel between the Gaussian (RBF) kernel (with kernel width hyperparameter  $\sigma > 0$ ) and the Inverse Multi-Quadratic (IMQ) kernel [58] (with hyperparameter  $K > 0$ ). For the proposed method, we tune the marginal constraint regularization between MMD and squared-MMD regularizers. We detail the chosen hyperparameters and other experimental details in the supplementary material.

### 4.1 Synthetic Experiments

#### 4.1.1 Level set of distances between distributions

**Dataset and experimental setup.** Applications like generative modeling deal with optimization over parameter ( $\theta$ ) of the source distribution to match the target distribution. In such cases, it is desirable that the level sets of the distance function over the measures show lesser number of stationary points which are not global optima [9]. Similar to [9], we consider a model family for source distributions as  $\mathcal{F} = \{P_\theta = \frac{1}{2}(\delta_\theta + \delta_{-\theta}) : \theta \in [-1, 1] \times [-1, 1]\}$  and a fixed target distribution  $Q$  as  $P_{(2,2)} \notin \mathcal{F}$ . We show distances between  $P_\theta$  and  $Q$  on varying  $\theta$ . More details are in appendix Section G.1.

**Results.** Figure 1 presents level sets showing distances  $\{d(P_\theta, Q) : \theta \in [-1, 1] \times [-1, 1]\}$  where the distance  $d(\cdot, \cdot)$  is measured using MMD, 2-Wasserstein, GW-TV and the proposed approach (9) respectively. We observe that the level sets of MMD show spurious local minima. The level sets of Wasserstein (OT with no regularization) and GW-TV show more number of local maxima compared to the level sets with the proposed approach.

#### 4.1.2 Transport plan in outlier-setting

**Dataset and experimental setup.** The data is presented in Figure 2(a). Both the source and the target data points are clustered into two groups. Additionally, the last data point of the target data is an outlier. In this set-up, the transport plan between the source and target is expected to have a block diagonal structure with the last column as all zeros.

**Compared Methods.** We compare the transport plan matrices of Wasserstein (OT with no regularization), Robust-OT (ROT) [5], GW-TV (OT with TV regularization), Robust-Semi-constrained Optimal Transport (RSOT) [33] and the proposed approach (9). ROT and RSOT are  $\phi$ -divergence based robust unbalanced OT formulations. ROT uses Chi-squared divergence regularization while RSOT uses KL regularization on one of the marginal constraints. More details are in appendix Section G.1.

**Results.** We qualitatively evaluate the transport plans in Figure 2. We observe that the transport plan matrix of the proposed approach (9) correctly captures the underlying structure and hence is robust to the outlier. The transport plan

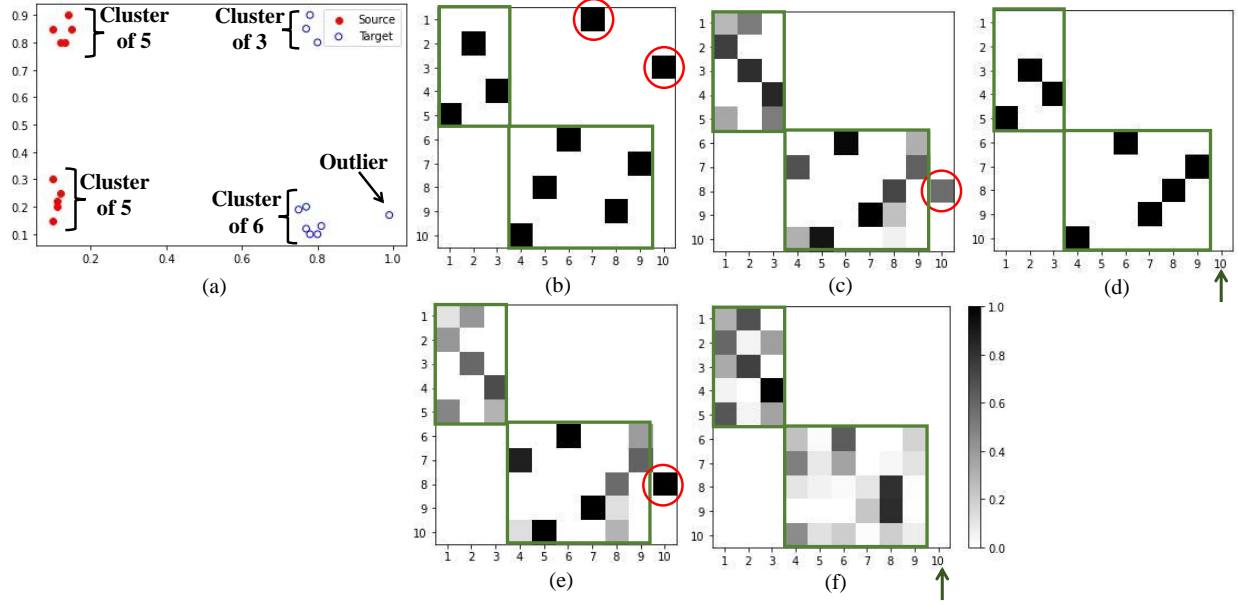


Figure 2: (a) Both the source and the target data are clustered into two groups and the target has an additional outlier. Plots (b), (c), (d), (e), and (f) are the transport plans learned using OT with no regularization, ROT, GW-TV, RSOT, and our approach (9) respectively. Plans (d) and (f) leave the outlier uncoupled (green arrow), and have the expected block diagonal structure (outlined in green). The plot (d) leaves even the non-outlier points uncoupled, hence, the proposed (d) is the most suitable here.

matrices of OT with no regularization, ROT, and SROT fail to handle the outlier. On the other hand, while the transport plan matrix of GW-TV shows some block-diagonal structure, it leaves even the non-outlier points uncoupled. Only the transport plan obtained by the proposed method shows separation between the outlier point and the rest.

## 4.2 Single cell RNA sequencing

Single cell RNA sequencing technique (scRNA-seq) provides insights into cellular functionality by recording expression profiles of genes [32, 64]. An expression profile is a mathematical expression of cells as vectors in gene expression space, where each dimension corresponds to gene. scRNA-seq helps us understand how the expression profile of the cells change over stages [52]. A population of cells is represented as a measure on the gene expression space and as they grow/divide/die and the measure evolves over time. While scRNA-seq records such a measure at a time stamp, it does so by destroying the cells [52]. Thus, it is not possible to monitor how the cell population evolve continuously over time. In fact, only a few measurements at discrete timesteps are generally taken due to the cost involved. Barycenter estimation in the OT framework offers a principled approach to estimate the trajectory of a measure at an intermediate timestep  $t$  ( $t_i < t < t_j$ ) when we have measurements available only at  $t_i$  (source) and  $t_j$  (target) time steps.

**Dataset and experimental setup.** We perform experiments on the Embryoid Body (EB) single-cell dataset [40]. The dataset has samples available at five timesteps ( $t_j$  with  $j = 0, \dots, 4$ ) which were collected during a 25-day period of development of human embryo. Following [61], we project the data onto two-dimensional space and associate uniform measures to the source and the target samples given at different timesteps. We consider the samples at timestep  $t_i$  and  $t_{i+2}$  as the samples from the source and target measures where  $0 \leq i \leq 2$  and aim at estimating the measure at  $t_i$  timestep as their barycenter with equal interpolation weights  $\rho_1 = \rho_2 = 0.5$ .

**Compared methods.** The barycenter of the measures are computed using the proposed MMD-UOT (12) and the  $\epsilon$ KL-UOT [11, 37] approaches. For both, simplex constraint is used to cater to the case of uniform measures. We also compare against the empirical average of the source and target measures which is the barycenter obtained with the MMD metric.

**Evaluation protocol.** The computed barycenter is evaluated against the measure corresponding to the ground truth samples available at the corresponding timestep. We compute the distance between two using the Earth Mover Distance (EMD). The hyperparameters are chosen based on leave-one-out validation protocol. More details are in appendix Section G.2.



Table 1: EMD (lower is better) between computed barycenter and ground truth distribution

TIMESTEP	MMD	$\epsilon$ KL-UOT	PROPOSED
T1	0.045	0.028	<b>0.020</b>
T2	0.012	<b>0.011</b>	<b>0.011</b>
T3	0.009	0.018	<b>0.008</b>

**Results.** We observe in Table 1 that the proposed approach performs better than the baselines on all the timesteps, suggesting its superior quality of interpolation.

### 4.3 Class ratio estimation

We next consider the class ratio estimation problem [31]. Given a multi-class labeled training dataset  $L := \{x_i, y_i\}_{i=1}^{m_1}$ , the aim is to estimate the ratio of classes in an unlabeled test dataset  $U := \{x_j\}_{j=m_1+1}^{m_2}$  (in the same input/output space). Here,  $x \in \mathbb{R}^d$  and  $y \in Y$ , where  $Y = \{1, \dots, c\}$  is the set of all labels. It should be noted that the distribution of classes in the labeled dataset may be different from the unlabeled dataset. Thus, while  $P_L(y) \neq P_U(y)$ , following existing works [65, 31], we assume that  $P(x|y)$  remains unchanged across datasets. Let's assume an unknown  $\theta \in \Delta_c$ , where  $\Delta_c := \{z \in \mathbb{R}^c | z \geq \mathbf{0}; \sum_i z_i = 1\}$ , is the class ratio in the test dataset, i.e.,  $P_U(y) = \theta$ . Then, a distribution  $Q(x) = \sum_{i=1}^c P_L(x|y=i)\theta_i$  should match the test distribution  $P_U(x)$ .

Existing works [65, 31] use IPMs such as MMD to learn the distribution  $\theta$ . For solving the class ratio estimation problem with MMD, the formulation is

$$\min_{\theta \in \Delta_c} \frac{1}{m_2} \mathbf{1}^\top G_{11} \mathbf{1} + z(\theta)^\top G_{22} z(\theta) - 2 \frac{1}{m_2} \mathbf{1}^\top G_{12} z(\theta),$$

where  $z(\theta) \in \mathbb{R}^{m_1}$ ,  $z_i(\theta) = \frac{\theta_{y_i}}{n_{y_i}}$ , and  $n_j$  denotes the number of instances labeled  $j$  in  $L$  and we denote the Gram matrices over the test data and the train data as  $G_{11}, G_{22}$  respectively.  $G_{12}$  denotes the kernel matrix between the test and train data.

To estimate the class ratios, we employ OT-based metrics with source as the unlabeled test data and target as the labeled train data. A key advantage of IPM-based regularization over KL-based regularization is flexibility in parameterization for estimation. Taking support of the transport matrix as the union of source and target data, we employ the proposed MMD regularized UOT formulation as follows:

$$\min_{\theta \in \Delta_c} \min_{\alpha \in S_1} \text{Tr}(\alpha \mathcal{C}^\top) + \lambda \{ \mathbf{1}^\top \alpha^\top G \alpha \mathbf{1} + \frac{1}{m_2} \mathbf{1}^\top G_{11} \mathbf{1} - 2 \frac{1}{m_2} \mathbf{1}^\top [G_{11} G_{12}] \alpha \mathbf{1} \} + \lambda \{ \mathbf{1}^\top \alpha G \alpha^\top \mathbf{1} + z(\theta)^\top G_{22} z(\theta) - 2 z(\theta)^\top [G_{21} G_{22}] \alpha^\top \mathbf{1} \},$$

where  $S_1 = \{\alpha \in \mathbb{R}^{m \times m}, \alpha \geq \mathbf{0}, \mathbf{1}^\top \alpha \mathbf{1} = 1\}$ ,  $\mathcal{C}$  and  $G$  are the cost and the Gram matrices, respectively, over the union of source and target data. The  $\epsilon$ KL-UOT formulation for class-ratio estimation problem is as follows:

$$\min_{\theta \in \Delta_c} \min_{\alpha \in S_2} \text{Tr}(\alpha \mathcal{C}_2^\top) + \lambda KL(\alpha \mathbf{1}, \frac{1}{m_2} \mathbf{1}) + \lambda KL(\alpha^\top \mathbf{1}, z(\theta)) + \epsilon \sum_{i=1}^{m_1} \sum_{j=1}^{m_2} \alpha_{i,j} \log \alpha_{i,j},$$

where  $S_2 = \{\alpha \in \mathbb{R}^{m_1 \times m_2}, \alpha \geq \mathbf{0}, \mathbf{1}^\top \alpha \mathbf{1} = 1\}$ .

**Dataset and experimental setup.** We follow the experimental setup described in [31] and show results on four binary classification datasets from the UCI repository [20]. The fraction of positive class examples on the training set is fixed as 0.5. For each dataset, we create four test set with the fraction of positive class examples as [0.2, 0.4, 0.6, 0.8].

**Evaluation protocol.** We report the average absolute deviation of the predicted class-ratios from the ground truth. We randomly generate train and test sets, where, for every train set, four test sets are generated corresponding to the four test class-ratios. Hyperparameters are tuned separately for each class ratio using 30 validation sets that were randomly sampled from the training set. More details are in appendix Section G.4.

**Results.** We report results in Table 2, averaged over four random splits. We observe that the proposed approach performs better than baselines on most datasets.

### 4.4 Domain adaptation in JUMBOT framework

OT has been widely employed in domain adaptation problems [16, 15, 53, 19]. JUMBOT [22] is a popular domain adaptation method based on  $\epsilon$ KL-UOT. JUMBOT's loss function involves a cross entropy term and  $\epsilon$ KL-UOT dis-

Table 2: Average mean absolute deviation (lower is better) obtained in class-ratio estimation experiments

DATASET	MMD	$\epsilon$ KL-UOT	PROPOSED
SAHEART	0.169 $\pm$ 0.059	0.102 $\pm$ 0.042	<b>0.085<math>\pm</math>0.054</b>
DIABETES	0.171 $\pm$ 0.029	0.134 $\pm$ 0.069	<b>0.112<math>\pm</math>0.072</b>
AUSTRALIAN	0.175 $\pm$ 0.018	0.114 $\pm$ 0.011	<b>0.089<math>\pm</math>0.018</b>
IONOSPHERE	<b>0.106<math>\pm</math>0.027</b>	0.212 $\pm$ 0.013	0.116 $\pm$ 0.061
GERMAN	0.198 $\pm$ 0.008	0.214 $\pm$ 0.106	<b>0.167<math>\pm</math>0.035</b>

Table 3: Target accuracy (higher is better) obtained in domain adaptation experiments

SOURCE	TARGET	$\epsilon$ KL-UOT	PROPOSED
SVHN	USPS	95.32	<b>96.21</b>
M-MNIST	USPS	93.57	<b>94.27</b>
SVHN	M-MNIST	93.55	<b>94.62</b>
MNIST	M-MNIST	96.71	<b>97.54</b>
SVHN	MNIST	98.67	<b>98.83</b>
USPS	MNIST	<b>98.57</b>	98.42
VISDA TRAIN	VISDA VAL	70.9	<b>72.2</b>

crepancy term between the source and target distributions. We showcase the utility of our MMD-regularized UOT formulation (9) in the JUMBOT [22] framework.

**Dataset and experimental setup** We perform the domain adaptation experiment with VisDA 2017 [48] and Digits datasets comprising of MNIST [34], M-MNIST [25], SVHN [46], USPS [30] datasets. We replace the  $\epsilon$ KL-UOT based loss with the proposed MMD-regularized UOT loss (9), keeping the other experimental set-up same as JUMBOT. We obtain JUMBOT’s result with  $\epsilon$ KL-UOT with the best reported hyperparameters [22]. Following JUMBOT, we tune our (MMD-regularized UOT loss) hyperparameters for the Digits experiment on USPS to MNIST (U $\rightarrow$ M) domain adaptation task and use the same hyperparameters for rest of the domain adaptation tasks on Digits. Following JUMBOT, we report validation accuracy on VisDA 2017. More details are in appendix Section G.3.

**Results** Table 3 reports the accuracy obtained on target datasets. We observe that our MMD-regularized UOT loss performs better than  $\epsilon$ KL-UOT based loss on six out of seven datasets.

#### 4.5 Two-sample hypothesis test

Given two sets of samples  $\{x_1, \dots, x_m\} \sim s$  and  $\{y_1, \dots, y_m\} \sim t$ , the aim of two-sample test is to determine whether the two sets of samples are drawn from the same distributions, viz., to predict if  $s = t$ . The performance evaluation in the two-sample test relies on two types of errors. Type-I error occurs when  $s = t$  but the algorithm predicts otherwise. Type-II error occurs when the algorithm incorrectly predicts  $s = t$ . The probability of Type-I error is called the significance level. The significance level can be controlled using permutation test based setups [21, 38]. Algorithms are typically compared based on the empirical estimate of their test power (higher is better), which is defined as the probability of not making a Type-II error, and the average Type-I error (lower is better).

**Dataset and experimental setup.** Following [38], we consider the two sets of samples one from the true MNIST [35] and another from fake MNIST generated by the DCGAN [7]. The data lies in 1024 dimensions. We take increasing number of samples ( $N$ ) and compute the average test power over 100 pairs of sets for each value of  $N$ . We repeat the experiment 10 times and report the average test power in Table 4 and the average Type-I error in Table 5 for the significance level  $\alpha = 0.05$ . We detail the procedure for choosing the hyperparameters and list of chosen hyperparameters for each method in appendix Section G.5.

**Results.** We observe in Table 4 that the test power of our method is the highest across all values of  $N$ . In Table 5, we also show that our Type-I error decays to 0 much faster compared to the that of the baseline methods.

## 5 Conclusion

The OT literature seems to have an overwhelming number of results with  $\phi$ -divergence based regularization. In comparison, IPM based regularization has received hardly any attention. We proposed a novel family of IPM-regularized

Table 4: Average Test Power (higher is better) on MNIST

N	MMD	$\epsilon$ KL-UOT	PROPOSED
20	0.064	0.067	<b>0.073</b>
40	0.076	0.084	<b>0.089</b>
60	0.081	0.086	<b>0.093</b>
80	0.065	0.095	<b>0.121</b>
100	0.101	0.096	<b>0.137</b>
200	0.121	0.174	<b>0.271</b>
300	0.204	0.227	<b>0.392</b>
400	0.264	0.288	<b>0.504</b>

Table 5: Average Type-I error (lower is better) on MNIST

N	MMD	$\epsilon$ KL-UOT	PROPOSED
20	<b>0.038</b>	0.063	0.046
40	0.050	0.044	<b>0.037</b>
60	0.035	0.045	<b>0.029</b>
80	0.034	0.028	<b>0.012</b>
100	0.036	0.030	<b>0.007</b>
200	0.021	0.016	<b>0</b>
300	0.011	0.003	<b>0</b>
400	0.004	0.003	<b>0</b>

OT formulations and investigated them both theoretically and empirically. Under mild conditions, we proved that they induce valid metrics and inherit useful properties from the parent metrics. Results on several applications showed that IPM-regularizers are indeed viable alternatives to the popular  $\phi$ -divergence based regularization in OT. We hope our results will motivate further study in this direction.

## References

- [1] Rohit Agrawal and Thibaut Horel. Optimal bounds between f-divergences and integral probability metrics. In *Proceedings of the 37th International Conference on Machine Learning*, 2020.
- [2] Martial Agueh and Guillaume Carlier. Barycenters in the wasserstein space. *SIAM Journal on Mathematical Analysis*, 43(2):904–924, 2011.
- [3] Jason Altschuler, Francis Bach, Alessandro Rudi, and Jonathan Niles-Weed. Massively scalable Sinkhorn distances via the Nystrom method. In *NeurIPS*, 2019.
- [4] Jason Altschuler, Jonathan Weed, and Philippe Rigollet. Near-linear time approximation algorithms for optimal transport via Sinkhorn iteration. In *NeurIPS*, 2017.
- [5] Yogesh Balaji, Rama Chellappa, and Soheil Feizi. Robust optimal transport with applications in generative modeling and domain adaptation. In H. Larochelle, M. Ranzato, R. Hadsell, M.F. Balcan, and H. Lin, editors, *Advances in Neural Information Processing Systems*, volume 33, pages 12934–12944. Curran Associates, Inc., 2020.
- [6] Amir Beck and Marc Teboulle. A fast iterative shrinkage-thresholding algorithm for linear inverse problems. *SIAM Journal on Imaging Sciences*, 2(1):183–202, 2009.
- [7] Yuemin Bian, Junmei Wang, Jaden Jungho Jun, and Xiang-Qun Xie. Deep convolutional generative adversarial network (dcgan) models for screening and design of small molecules targeting cannabinoid receptors. *Molecular Pharmaceutics*, 16(11):4451–4460, 2019.
- [8] Radu Ioan Bot. *Conjugate Duality in Convex Optimization*, volume 637 of *Lecture Notes in Economics and Mathematical Systems book series*. Springer, 2010.
- [9] Leon Bottou, Martin Arjovsky, David Lopez-Paz, and Maxime Oquab. Geometrical insights for implicit generative modeling. *arXiv preprint arXiv:1712.07822*, 2017.
- [10] Stephen Boyd and Lieven Vandenberghe. *Convex optimization*. Cambridge university press, 2004.

- [11] L. Chizat, G. Peyré, B. Schmitzer, and F.-X. Vialard. Unbalanced optimal transport: Dynamic and kantorovich formulations. *Journal of Functional Analysis*, 274(11):3090–3123, 2018.
- [12] Lenaïc Chizat. Unbalanced optimal transport : Models, numerical methods, applications. Technical report, Universite Paris sciences et lettres, 2017.
- [13] Lenaïc Chizat, Gabriel Peyré, Bernhard Schmitzer, and François-Xavier Vialard. Scaling algorithms for unbalanced optimal transport problems. *Math. Comput.*, 87(314):2563–2609, 2018.
- [14] Patrick L. Combettes, Andrew M. McDonald, Charles A. Micchelli, and Massimiliano Pontil. Learning with optimal interpolation norms. *Numerical Algorithms*, 81:695–717, 2018.
- [15] N. Courty, R. Flamary, D. Tuia, and A. Rakotomamonjy. Optimal transport for domain adaptation. *IEEE Transactions on Pattern Analysis and Machine Intelligence*, 39(9):1853–1865, 2017.
- [16] Nicolas Courty, Rémi Flamary, Amaury Habrard, and Alain Rakotomamonjy. Joint distribution optimal transportation for domain adaptation. In *Advances in Neural Information Processing Systems*, volume 30, pages 3730–3739, 2017.
- [17] Marco Cuturi. Sinkhorn distances: Lightspeed computation of optimal transport. In *Proceedings of the 26th International Conference on Neural Information Processing Systems - Volume 2*, page 2292–2300, 2013.
- [18] Marco Cuturi and Arnaud Doucet. Fast computation of wasserstein barycenters. In *Proceedings of the 31st International Conference on International Conference on Machine Learning - Volume 32*, page II–685–II–693. JMLR.org, 2014.
- [19] Bharath Bhushan Damodaran, Benjamin Kellenberger, Rémi Flamary, Devis Tuia, and Nicolas Courty. Deepjdot: Deep joint distribution optimal transport for unsupervised domain adaptation, 2018.
- [20] Dheeru Dua and Casey Graff. UCI machine learning repository, 2017.
- [21] Michael D. Ernst. Permutation Methods: A Basis for Exact Inference. *Statistical Science*, 19(4):676 – 685, 2004.
- [22] Kilian Fatras, Thibault Séjourné, Nicolas Courty, and Rémi Flamary. Unbalanced minibatch optimal transport; applications to domain adaptation. In *Proceedings of the 38th International Conference on Machine Learning*, 2021.
- [23] Jean Feydy, Thibault Séjourné, François-Xavier Vialard, Shun-ichi Amari, Alain Trounev, and Gabriel Peyré. Interpolating between optimal transport and mmd using sinkhorn divergences. In *AISTATS*, 2019.
- [24] Charlie Frogner, Chiyuan Zhang, Hossein Mobahi, Mauricio Araya-Polo, and Tomaso Poggio. Learning with a wasserstein loss. In *Proceedings of the 28th International Conference on Neural Information Processing Systems - Volume 2*, pages 2053–2061, 2015.
- [25] Yaroslav Ganin, Evgeniya Ustinova, Hana Ajakan, Pascal Germain, Hugo Larochelle, François Laviolette, Mario Marchand, and Victor Lempitsky. Domain-adversarial training of neural networks. *The journal of machine learning research*, 17(1):2096–2030, 2016.
- [26] Aude Genevay, Lénaïc Chizat, Francis Bach, Marco Cuturi, and Gabriel Peyré. Sample complexity of sinkhorn divergences. In *The 22nd International Conference on Artificial Intelligence and Statistics, AISTATS 2019, 16-18 April 2019, Naha, Okinawa, Japan*, pages 1574–1583, 2019.
- [27] Tryphon T. Georgiou, Johan Karlsson, and Mir Shahrouz Takyar. Metrics for power spectra: An axiomatic approach. *IEEE Transactions on Signal Processing*, 57(3):859–867, 2009.
- [28] Alexandre Gramfort, Gabriel Peyré, and Marco Cuturi. Fast optimal transport averaging of neuroimaging data. In *Proceedings of 24th International Conference on Information Processing in Medical Imaging*, 2015.
- [29] Leonid G. Hanin. Kantorovich-rubinstein norm and its application in the theory of lipschitz spaces. In *PROCEEDINGS OF THE AMERICAN MATHEMATICAL SOCIETY*, volume 115, 1992.
- [30] J.J. Hull. A database for handwritten text recognition research. *IEEE Transactions on Pattern Analysis and Machine Intelligence*, 16(5):550–554, 1994.
- [31] Arun Iyer, J. Saketha Nath, and Sunita Sarawagi. Maximum mean discrepancy for class ratio estimation. In *ICML*, 2014.
- [32] Aleksandra. A. Kolodziejczyk, Jong Kyoung Kim, Valentine Svensson, John. C. Marioni, and Sarah. A. Teichmann. The technology and biology of single-cell rna sequencing. *Molecular Cell*, 58(4):610–620, 2015.
- [33] Khang Le, Huy Nguyen, Quang M Nguyen, Tung Pham, Hung Bui, and Nhat Ho. On robust optimal transport: Computational complexity and barycenter computation. In M. Ranzato, A. Beygelzimer, Y. Dauphin, P.S. Liang, and J. Wortman Vaughan, editors, *Advances in Neural Information Processing Systems*, volume 34, pages 21947–21959. Curran Associates, Inc., 2021.

- [34] Yann LeCun and Corinna Cortes. MNIST handwritten digit database. <http://yann.lecun.com/exdb/mnist/>, 2010.
- [35] Yann LeCun and Corinna Cortes. MNIST handwritten digit database. 2010.
- [36] Matthias Liero, Alexander Mielke, and Giuseppe Savaré. Optimal transport in competition with reaction: The hellinger-kantorovich distance and geodesic curves. *SIAM J. Math. Anal.*, 48:2869–2911, 2016.
- [37] Matthias Liero, Alexander Mielke, and Giuseppe Savaré. Optimal entropy-transport problems and a new hellinger-kantorovich distance between positive measures. *Inventiones mathematicae*, 211(3):969–1117, 2018.
- [38] Feng Liu, Wenkai Xu, Jie Lu, Guangquan Zhang, Arthur Gretton, and Danica J. Sutherland. Learning deep kernels for non-parametric two-sample tests. In *ICML*, 2020.
- [39] Gonzalo Mena and Jonathan Niles-Weed. Statistical bounds for entropic optimal transport: sample complexity and the central limit theorem. In H. Wallach, H. Larochelle, A. Beygelzimer, F. d’Alché-Buc, E. Fox, and R. Garnett, editors, *Advances in Neural Information Processing Systems*, volume 32. Curran Associates, Inc., 2019.
- [40] Kevin R. Moon, David van Dijk, Zheng Wang, Scott Gigante, Daniel B. Burkhardt, William S. Chen, Kristina Yim, Antonia van den Elzen, Matthew J. Hirn, Ronald R. Coifman, Natalia B. Ivanova, Guy Wolf, and Smita Krishnaswamy. Visualizing structure and transitions for biological data exploration. *Nature Biotechnology*, 37(12):1482–1492, 2019.
- [41] Krikamol Muandet, Kenji Fukumizu, Bharath Sriperumbudur, and Bernhard Schölkopf. Kernel mean embedding of distributions: A review and beyond. *Foundations and Trends® in Machine Learning*, 10(1-2):1–141, 2017.
- [42] Alfred Muller. Integral probability metrics and their generating classes of functions. *Advances in Applied Probability*, 29:429–443, 1997.
- [43] J. Saketha Nath and Pratik Kumar Jawanpuria. Statistical optimal transport posed as learning kernel embedding. In *Advances in Neural Information Processing Systems*, 2020.
- [44] Yurii Nesterov. *Introductory lectures on convex optimization: A basic course*, volume 87. Springer Science & Business Media, 2003.
- [45] Yurii E Nesterov. A method for solving the convex programming problem with convergence rate  $O(1/k^2)$ . In *Dokl. akad. nauk Sssr*, volume 269, pages 543–547, 1983.
- [46] Yuval Netzer, Tiejie Wang, Adam Coates, A. Bissacco, Bo Wu, and A. Ng. Reading digits in natural images with unsupervised feature learning. In *NeurIPS*, 2011.
- [47] Jonathan Niles-Weed and Philippe Rigollet. Estimation of Wasserstein distances in the spiked transport model, 2019.
- [48] Xingchao Peng, Ben Usman, Neela Kaushik, Judy Hoffman, Dequan Wang, and Kate Saenko. Visda: The visual domain adaptation challenge. *arXiv preprint arXiv:1710.06924*, 2017.
- [49] Gabriel Peyré and Marco Cuturi. Computational optimal transport. *Foundations and Trends® in Machine Learning*, 11(5-6):355–607, 2019.
- [50] Benedetto Piccoli and Francesco Rossi. Generalized wasserstein distance and its application to transport equations with source. *Archive for Rational Mechanics and Analysis*, 211:335–358, 2014.
- [51] Benedetto Piccoli and Francesco Rossi. On properties of the generalized wasserstein distance. *Archive for Rational Mechanics and Analysis*, 222, 12 2016.
- [52] Geoffrey Schiebinger, Jian Shu, Marcin Tabaka, Brian Cleary, Vidya Subramanian, Aryeh Solomon, Joshua Gould, Siyan Liu, Stacie Lin, Peter Berube, Lia Lee, Jenny Chen, Justin Brumbaugh, Philippe Rigollet, Konrad Hochedlinger, Rudolf Jaenisch, Aviv Regev, and Eric S. Lander. Optimal-transport analysis of single-cell gene expression identifies developmental trajectories in reprogramming. *Cell*, 176(4):928–943.e22, 2019.
- [53] Vivien. Seguy, Bharath B. Damodaran, Remi Flamary, Nicolas Courty, Antoine Rolet, and Mathieu Blondel. Large-scale optimal transport and mapping estimation. In *International Conference on Learning Representations (ICLR)*, 2018.
- [54] Justin Solomon, Fernando de Goes, Gabriel Peyré, Marco Cuturi, Adrian Butscher, Andy Nguyen, Tao Du, and Leonidas Guibas. Convolutional wasserstein distances: Efficient optimal transportation on geometric domains. *ACM Trans. Graph.*, 34(4), 2015.
- [55] Justin Solomon, Raif Rustamov, Leonidas Guibas, and Adrian Butscher. Wasserstein propagation for semi-supervised learning. In Eric P. Xing and Tony Jebara, editors, *Proceedings of the 31st International Conference on Machine Learning*, volume 32 of *Proceedings of Machine Learning Research*, pages 306–314, 2014.
- [56] Bharath K. Sriperumbudur, Kenji Fukumizu, Arthur Gretton, Bernhard Schölkopf, and Gert R. G. Lanckriet. On integral probability metrics, phi-divergences and binary classification. *arXiv preprint arXiv:0901.2698*, 2009.

- [57] Bharath K. Sriperumbudur, Kenji Fukumizu, and Gert R. G. Lanckriet. Universality, characteristic kernels and RKHS embedding of measures. *Journal of Machine Learning Research*, 12:2389–2410, 2011.
- [58] Bharath K. Sriperumbudur, Kenji Fukumizu, and Gert R. G. Lanckriet. Universality, characteristic kernels and rkhs embedding of measures. *J. Mach. Learn. Res.*, 12(null):2389–2410, jul 2011.
- [59] Yanfeng Sun, Junbin Gao, Xia Hong, Bamdev Mishra, and Baocai Yin. Heterogeneous tensor decomposition for clustering via manifold optimization. *IEEE Transactions on Pattern Analysis and Machine Intelligence*, 38(3):476–489, 2016.
- [60] I. Tolstikhin, B. Sriperumbudur, and K. Muandet. Minimax estimation of kernel mean embeddings. arxiv, 2016.
- [61] Alexander Tong, Jessie Huang, Guy Wolf, David Van Dijk, and Smita Krishnaswamy. TrajectoryNet: A dynamic optimal transport network for modeling cellular dynamics. In Hal Daumé III and Aarti Singh, editors, *Proceedings of the 37th International Conference on Machine Learning*, volume 119 of *Proceedings of Machine Learning Research*, pages 9526–9536. PMLR, 13–18 Jul 2020.
- [62] C. Villani. *Topics in Optimal Transportation Theory*, volume 58 of *Graduate Studies in Mathematics*. American Mathematical Society, 01 2003.
- [63] Cédric Villani. *Optimal Transport: Old and New*. A series of Comprehensive Studies in Mathematics. Springer, 2009.
- [64] A. Wagner, A. Regev, and N. Yosef. Revealing the vectors of cellular identity with single-cell genomics. *Nature Biotechnology*, 34:1145–1160, 2016.
- [65] K. Zhang, B. Scholkopf, K. Muandet, and Z. Wang. Domain adaptation under target and conditional shift. In *ICML*, 2013.

## A Proof of Lemma 3.1

**Lemma A.1.**

$$(\mathcal{U}_{\mathcal{G},c,\lambda,p,q}(s_0, t_0))^q \equiv \min_{\pi \in \mathcal{R}^+(\mathcal{X} \times \mathcal{X})} \left( |\pi|^{p-1} \int c^p d\pi \right)^{q/p} + \lambda \gamma_{\mathcal{G}}^q(\pi_1, s_0) + \lambda \gamma_{\mathcal{G}}^q(\pi_2, t_0),$$

can be equivalently re-written in the following form:

$$(\mathcal{U}_{\mathcal{G},c,\lambda,p,q}(s_0, t_0))^q = \min_{s,t \in \mathcal{R}^+(\mathcal{X})} |s|^q (W_p(s, t))^q + \lambda \gamma_{\mathcal{G}}^q(s, s_0) + \lambda \gamma_{\mathcal{G}}^q(t, t_0),$$

$$\text{where } W_p(s, t) \equiv \begin{cases} \bar{W}_p\left(\frac{s}{|s|}, \frac{t}{|t|}\right) & \text{if } |s| = |t|, \\ \infty & \text{otherwise.} \end{cases}$$

*Proof.*

$$\begin{aligned} & \min_{s,t \in \mathcal{R}^+(\mathcal{X})} |s|^q W_p(s, t)^q + \lambda \gamma_{\mathcal{G}}^q(s, s_0) + \lambda \gamma_{\mathcal{G}}^q(t, t_0) \\ &= \min_{s,t \in \mathcal{R}^+(\mathcal{X}); |s|=|t|} |s|^q \min_{\bar{\pi} \in \mathcal{R}_1^+(\mathcal{X} \times \mathcal{X})} \left( \int c^p d\bar{\pi} \right)^{q/p} + \lambda \gamma_{\mathcal{G}}^q(s, s_0) + \lambda \gamma_{\mathcal{G}}^q(t, t_0) \text{ s.t. } \bar{\pi}_1 = \frac{s}{|s|}, \bar{\pi}_2 = \frac{t}{|t|} \\ &= \min_{\eta > 0} \eta^q \min_{\bar{\pi} \in \mathcal{R}_1^+(\mathcal{X} \times \mathcal{X})} \left( \int c^p d\bar{\pi} \right)^{q/p} + \lambda \gamma_{\mathcal{G}}^q(\eta \bar{\pi}_1, s_0) + \lambda \gamma_{\mathcal{G}}^q(\eta \bar{\pi}_2, t_0) \\ &= \min_{\eta > 0} \min_{\bar{\pi} \in \mathcal{R}_1^+(\mathcal{X} \times \mathcal{X})} \left( \eta^{p-1} \int c^p \eta d\bar{\pi} \right)^{q/p} + \lambda \gamma_{\mathcal{G}}^q(\eta \bar{\pi}_1, s_0) + \lambda \gamma_{\mathcal{G}}^q(\eta \bar{\pi}_2, t_0) \\ &= \min_{\pi \in \mathcal{R}^+(\mathcal{X} \times \mathcal{X})} \left( |\pi|^{p-1} \int c^p d\pi \right)^{q/p} + \lambda \gamma_{\mathcal{G}}^q(\pi_1, s_0) + \lambda \gamma_{\mathcal{G}}^q(\pi_2, t_0) \end{aligned}$$

The first equality holds from the definition of  $W_p$ . Eliminating normalized versions  $s$  and  $t$  using the equality constraints, and introducing  $\eta$  to denote their common mass gives the second equality. The last equality comes after changing the variable of optimization to  $\pi \in \mathcal{R}^+(\mathcal{X} \times \mathcal{X}) \equiv \eta \bar{\pi}$ . Recall that  $\mathcal{R}^+(\mathcal{X})$  denotes the set of all non-negative Radon measures defined over  $\mathcal{X}$ ; while the set of all probability measures is denoted by  $\mathcal{R}_1^+(\mathcal{X})$ .  $\square$

## B Proof of Theorem 3.2

We give a proof for Theorem 3.2 through Fenchel Duality and using the fact that IPM's are norm-induced metrics, i.e.,  $\gamma_{\mathcal{G}}(a, b) = \|a - b\|$  for some norm  $\|\cdot\|$ . Our proof uses the expression for conjugate of an arbitrary norm derived in the following lemma.

**Lemma B.1.** *The conjugate of  $\|\cdot\|^q$  where  $\|\cdot\|$  is an arbitrary norm and  $q > 1$ , is  $\alpha \|\cdot\|_*^r$  where  $\|\cdot\|_*$  is the Dual norm of  $\|\cdot\|$ ,  $\frac{1}{r} + \frac{1}{q} = 1$  and  $\alpha = \frac{q-1}{q^r}$ .*

*Proof.* Let  $\mathcal{V}$  be a vector space and consider an  $x \in \mathcal{V}$  such that  $x \neq 0$ . We denote  $f^c$  as the conjugate of the function  $f$ .

$$\begin{aligned} (\|x\|^q)^c &= \max_{y \in \mathcal{V}} \langle x, y \rangle - \|y\|^q \\ &= \max_{t \in \mathbb{R}} \max_{y \in \mathcal{V}; t \geq \|y\|} \langle x, y \rangle - t^q \text{ (Using the Epigraph trick)} \\ &= \max_{t > 0} \max_{\frac{y}{t} \in \mathcal{V}; \|\frac{y}{t}\| \leq 1} t \left\langle x, \frac{y}{t} \right\rangle - t^q \\ &= \max_{t > 0} t \|x\|_* - t^q \\ &= \alpha \|x\|_*^r \end{aligned}$$

$\square$

We now prove the Theorem 3.2.

*Proof.*

$$\begin{aligned}
\mathcal{U}_{\mathcal{G},c,\lambda,1,q}(s_0, t_0)^q &= \min_{s,t \in \mathcal{R}^+(\mathcal{X})} |s|^q W_1^q(s, t) + \lambda \gamma_{\mathcal{G}}^q(s, s_0) + \lambda \gamma_{\mathcal{G}}^q(t, t_0) \\
&= \min_{s,t \in \mathcal{R}^+(\mathcal{X}); |s|=|t|} |s|^q \bar{W}_1^q\left(\frac{s}{|s|}, \frac{t}{|t|}\right) + \lambda \gamma_{\mathcal{G}}^q(s, s_0) + \lambda \gamma_{\mathcal{G}}^q(t, t_0) \\
&= \min_{s,t \in \mathcal{R}^+(\mathcal{X}); |s|=|t|} \bar{W}_1^q(s, t) + \lambda \gamma_{\mathcal{G}}^q(s, s_0) + \lambda \gamma_{\mathcal{G}}^q(t, t_0) \\
&= \min_{s,t \in \mathcal{R}^+(\mathcal{X}); |s|=|t|} \|s - t\|^q + \lambda \|s - s_0\|_{\gamma}^q + \lambda \|t - t_0\|_{\gamma}^q \text{ (where } \|\cdot\| \text{ is the Kantorovich norm and } \|\cdot\|_{\gamma} \\
&\quad \text{is the norm corresponding to } \gamma_{\mathcal{G}}) \\
&= \min_{s,t \in \mathcal{R}^+(\mathcal{X}); |s|=|t|} \max_{f_1 \in \mathcal{F}} (\langle f_1, s - t \rangle - \alpha \|f_1\|_*^r) + \lambda \max_{f \in \mathcal{F}} (\langle f, s - s_0 \rangle - \alpha \|f\|_{*\gamma}^r) + \\
&\quad \lambda \max_{g \in \mathcal{F}} (\langle g, t - t_0 \rangle - \alpha \|g\|_{*\gamma}^r) \text{ (Using Lemma B.1)}
\end{aligned}$$

Then, using Sion min-max exchange Theorem <sup>4</sup>, we get,

$$\begin{aligned}
\mathcal{U}_{\mathcal{G},c,\lambda,1,q}(s_0, t_0)^q &= \max_{f_1, f, g \in \mathcal{F}} \min_{s,t \in \mathcal{R}^+(\mathcal{X}); |s|=|t|} \langle f_1 + \lambda f, s \rangle + \langle \lambda g - f_1, t \rangle - \alpha (\|f_1\|_*^r + \lambda \|f\|_{*\gamma}^r + \lambda \|g\|_{*\gamma}^r) - \\
&\quad \lambda (\langle f, s_0 \rangle + \langle g, t_0 \rangle)
\end{aligned}$$

We note that

$$\min_{s,t \in \mathcal{R}^+(\mathcal{X}); |s|=|t|} \langle f_1 + \lambda f, s \rangle + \langle \lambda g - f_1, t \rangle = \begin{cases} 0 & \text{if } -\lambda f \leq f_1 \leq \lambda g, \\ -\infty & \text{otherwise.} \end{cases}$$

Also, as the dual norm  $\|\cdot\|_*^r$  is a valid norm and hence an increasing function,

$$\begin{aligned}
\min_{f_1 \in \mathcal{F}; -\lambda f \leq f_1 \leq \lambda g} \|f_1\|_*^r &= \|\lambda f\|_*^r \text{ (which is achieved at } f_1 = -\lambda f) \\
\min_{g \in \mathcal{F}; g \geq -f} \lambda (\alpha \|g\|_{*\gamma}^r + \langle g, t_0 \rangle) &= \lambda (\alpha \|f\|_{*\gamma}^r + \langle -f, t_0 \rangle) \text{ } (\because t_0 \in \mathcal{R}^+(\mathcal{X}))
\end{aligned}$$

After eliminating  $f_1$  and  $g$  using the above, we get

$$\begin{aligned}
\mathcal{U}_{\mathcal{G},c,\lambda,1,q}(s_0, t_0) &= \left( \max_{f \in \mathcal{F}} -\alpha \|\lambda f\|_*^r + \lambda \langle f, t_0 - s_0 \rangle - 2\alpha \lambda \|f\|_{*\gamma}^r \right)^{\frac{1}{q}} \\
&= \left( \max_{f \in \mathcal{F}} \langle f, t_0 - s_0 \rangle - \frac{2\alpha}{\lambda^{r-1}} \|f\|_{*\gamma}^r - \alpha \|f\|_*^r \right)^{\frac{1}{q}} \\
&= \left( \min_{\mu, \nu \in \mathcal{F}; \mu + \nu = t_0 - s_0} \left( \frac{2\alpha \|\mu\|_{*\gamma}^r}{\lambda^{r-1}} \right)^c + (\alpha \|\nu\|_*^r)^c \right)^{\frac{1}{q}} \\
&= \left( \min_{\mu, \nu \in \mathcal{F}; \mu + \nu = t_0 - s_0} \frac{\eta \lambda}{(2\alpha)^{q-1}} \|\mu\|_{\gamma}^q + \frac{\eta}{\alpha^{q-1}} \|\nu\|_{\gamma}^q \right)^{\frac{1}{q}} \text{ (Using Lemma B.1)} \\
&\quad \text{where } \eta = \frac{r-1}{r^q}
\end{aligned}$$

The above  $q$ -degree infimal convolution form is an interpolation norm defined in equation (2.21) in [14]. We conclude that  $\mathcal{U}_{\mathcal{G},c,\lambda,1,q}(s_0, t_0)$  is an interpolation norm between Kantorovich norm and the norm corresponding to the Dual norm regularization, and hence a norm-induced metric. To the best of our knowledge, this is a novel family of norms induced over measures.  $\square$

## C Proof of Theorem 3.4

We present a proof based on the classical Moreau-Rockafellar formula [8]:

<sup>4</sup>our regularization ensures that the problem is bounded



**Theorem C.1.** Let  $X$  be a real Banach space and  $f, g : X \mapsto \mathbb{R} \cup \{\infty\}$  be closed convex functions such that  $\text{dom}(f) \cap \text{dom}(g)$  is not empty, then:  $(f + g)^*(y) = \min_{x_1 + x_2 = y} f^*(x_1) + g^*(x_2) \forall y \in X^*$ . Here,  $f^*$  is the Fenchel conjugate of  $f$  and  $X^*$  is the topological dual space of  $X$ .

*Proof.* Consider the indicator function  $F_c : \mathcal{C}(\mathcal{X} \times \mathcal{X}) \mapsto \mathbb{R} \cup \{\infty\}$  defined by:  $F_c(f, g) = 0$  if  $f(x) + g(y) \leq c(x, y) \forall x, y \in \mathcal{X}$ , and  $\infty$  otherwise. Consider another indicator function:  $F_{\mathcal{G}}(f, g)$  defined as: 0 if  $f \in \mathcal{G}, g \in \mathcal{G}$  and  $\infty$  otherwise. Topological dual of  $\mathcal{C}(\mathcal{X} \times \mathcal{X})$  is regular Radon measures  $\mathcal{R}(\mathcal{X} \times \mathcal{X})$  and the duality product  $\langle h, \pi \rangle \equiv \int h d\pi$ .

Now, it is easy to see that  $F_c^*(s, t) = \max_{f \in \mathcal{C}(\mathcal{X}), g \in \mathcal{C}(\mathcal{X})} \int f ds + \int g dt$ , s.t.  $f(x) + g(y) \leq c(x, y) \forall x, y \in \mathcal{X}$ , which under the assumptions that  $\mathcal{X}$  is compact and  $c$  is continuous, is Wasserstein  $W(s, t)$  with cost  $c$  [62]. On the other hand,  $F_{\mathcal{G}(\lambda)}^*(s, t) = \lambda (\max_{f \in \mathcal{G}} \int f ds + \max_{g \in \mathcal{G}} \int g dt) = \lambda (\gamma_{\mathcal{G}}(s, 0) + \gamma_{\mathcal{G}}(t, 0))$ . Note that  $\mathcal{U}_{\mathcal{G}, c, \lambda, 1, 1}(s_0, t_0) = \min_{(s, t) + (s_1, t_1) = (s_0, t_0)} F_c^*(s, t) + F_{\mathcal{G}(\lambda)}^*(s_1, t_1)$ .

Now, observe that  $F_{\mathcal{G}}$  is a closed, convex function because  $\mathcal{G}$  is a closed, convex set. On the other hand,  $F_c$  is trivially convex and is closed because  $c$  is continuous. Hence by applying the Moreau-Rockafellar formula we have that:

$$\mathcal{U}_{\mathcal{G}, c, \lambda, 1, 1}(s_0, t_0) = \max_{f \in \mathcal{G}(\lambda), g \in \mathcal{G}(\lambda)} \int f ds + \int g dt, \text{ s.t. } f(x) + g(y) \leq c(x, y) \forall x, y \in \mathcal{X} \quad (13)$$

Now, the constraints in (13) are equivalent to:  $g(y) \leq \min_{x \in \mathcal{X}} c(x, y) - f(x) \forall y \in \mathcal{X}$ . The RHS is nothing but the  $c$ -conjugate ( $c$ -transform) of  $f$ . From proposition 6 in [49], whenever  $c$  is a metric, we have:  $\min_{x \in \mathcal{X}} d(x, y) - f(x) = \begin{cases} -f(y) & \text{if } f \in \mathcal{W}_c, \\ -\infty & \text{otherwise.} \end{cases}$  Thus the constraints are equivalent to:  $g(y) \leq -f(y) \forall y \in \mathcal{X}, f \in \mathcal{W}_c$ . By symmetry, we also obtain that  $f(y) \leq -g(y) \forall y \in \mathcal{X}, g \in \mathcal{W}_c$ . Now, since the dual, (13), seeks to maximize the objective with respect to  $g$ , and monotonically increases with values of  $g$ ; at optimality we have that  $g(y) = -f(y) \forall y \in \mathcal{X}$ . Note that this equality is possible to achieve as both  $g, f \in \mathcal{G}(\lambda) \cap \mathcal{W}_c$ . Eliminating  $g$ , one obtains (7).  $\square$

## D Proof of Theorem 3.7

As per 6,  $\mathcal{U}_{\mathcal{G}, c, \lambda, p, p}^p = \min_{s, t \in \mathcal{R}_1^+(\mathcal{X})} h(s, t, s_0, t_0)$ , where  $h(x) = h_1(x) + h_2(x) + h_3(x)$ . Here,  $h_1$  is the  $W_p^p$  term,  $h_2, h_3$  are the IPM-regularizer terms raised to power  $p$ .  $h_1$  is convex according to theorem 4.8 in [63].  $h_2, h_3$  are convex as IPMs are norm-induced metrics and  $p > 1$ . Therefore,  $h$  is a convex function. From basic convexity results (e.g., section 3.2.5 in [10]), it follows that,  $\mathcal{U}_{\mathcal{G}, c, \lambda, p, p}^p$ , which is a partial minimization of  $h$ , is convex.

## E More on Additional Properties 3.3

### E.1 Proof of Sample Complexity Theorem 3.8

**Theorem E.1.** Let  $\lambda > 0, p \geq 1, q \geq 1$ . Let us denote  $\mathcal{U}_{\mathcal{G}, c, \lambda, p, q}$ , defined in (5), by  $\bar{\mathcal{U}}_q$ . Let  $\hat{s}_m, \hat{t}_m$  denote the empirical estimates of  $s_0, t_0$  respectively with  $m$  samples. Then,  $\bar{\mathcal{U}}_1(\hat{s}_m, \hat{t}_m) \rightarrow \bar{\mathcal{U}}_1(s_0, t_0)$  at a rate same as that of  $\gamma_{\mathcal{G}}(\hat{s}_m, s_0) \rightarrow 0$ . Further,  $\bar{\mathcal{U}}_q^q(\hat{s}_m, \hat{t}_m) \rightarrow \bar{\mathcal{U}}_q^q(s_0, t_0)$  at a rate same as that of  $\gamma_{\mathcal{G}}(\hat{s}_m, s_0) \rightarrow 0$ .

Recalling the definition of  $\bar{\mathcal{U}}_q$ :

$$\bar{\mathcal{U}}_q(s_0, t_0) \equiv \min_{\pi \in \mathcal{R}^+(\mathcal{X} \times \mathcal{X})} h(\pi, s_0, t_0) \equiv \left( \left( \int c^p d\pi \right)^{q/p} + \lambda \gamma_{\mathcal{G}}^q(\pi_1, s_0) + \lambda \gamma_{\mathcal{G}}^q(\pi_2, t_0) \right)^{\frac{1}{q}},$$

**Case:**  $q = 1$

$$\begin{aligned} \bar{\mathcal{U}}_1(\hat{s}_m, \hat{t}_m) - \bar{\mathcal{U}}_1(s_0, t_0) &= \min_{\pi \in \mathcal{R}^+(\mathcal{X} \times \mathcal{X})} h(\pi, \hat{s}_m, \hat{t}_m) - \min_{\pi \in \mathcal{R}^+(\mathcal{X} \times \mathcal{X})} h(\pi, s_0, t_0) \\ &\leq h(\pi^*, \hat{s}_m, \hat{t}_m) - h(\pi^*, s_0, t_0) \left( \text{where } \pi^* = \arg \min_{\pi \in \mathcal{R}^+(\mathcal{X} \times \mathcal{X})} h(\pi, s_0, t_0) \right) \\ &= \lambda (\gamma_{\mathcal{G}}(\pi_1^*, \hat{s}_m) - \gamma_{\mathcal{G}}(\pi_1^*, s_0) + \gamma_{\mathcal{G}}(\pi_2^*, \hat{t}_m) - \gamma_{\mathcal{G}}(\pi_2^*, t_0)) \\ &\leq \lambda (\gamma_{\mathcal{G}}(s_0, \hat{s}_m) + \gamma_{\mathcal{G}}(t_0, \hat{t}_m)) \quad (\because \gamma \text{ satisfies triangle inequality}) \end{aligned} \quad (14)$$

Similarly, one can show that

$$- (\bar{\mathcal{U}}_1(\hat{s}_m, \hat{t}_m) - \bar{\mathcal{U}}_1(s_0, t_0)) \leq \lambda (\gamma_{\mathcal{G}}(s_0, \hat{s}_m) + \gamma_{\mathcal{G}}(t_0, \hat{t}_m)) \quad (15)$$

From 14 and 15,  $|\bar{\mathcal{U}}_1(\hat{s}_m, \hat{t}_m) - \bar{\mathcal{U}}_1(s_0, t_0)| \leq \lambda (\gamma_{\mathcal{G}}(s_0, \hat{s}_m) + \gamma_{\mathcal{G}}(t_0, \hat{t}_m))$ .

**Case:**  $q > 1$  We use the following lemma in our proof for the case  $q > 1$

**Lemma E.2.** Consider  $\bar{M}(s_0, t_0) \equiv \max_{s \in \mathcal{R}_1^+(\mathcal{X})} \gamma_{\mathcal{G}}(s, s_0) + \gamma_{\mathcal{G}}(s, t_0) < \infty \forall s_0, t_0 \in \mathcal{R}_1^+(\mathcal{X})$ .

$\bar{M}(\hat{s}_m, \hat{t}_m) \rightarrow \bar{M}(s_0, t_0)$  at a rate same as  $\gamma_{\mathcal{G}}(\hat{s}_m, \hat{t}_m) \rightarrow \gamma_{\mathcal{G}}(s_0, t_0)$ .

*Proof.*

$$\begin{aligned} |\bar{M}(s_0, t_0) - \bar{M}(\hat{s}_m, \hat{t}_m)| &= \left| \left( \max_{s \in \mathcal{R}_1^+(\mathcal{X})} \gamma_{\mathcal{G}}(s, s_0) + \gamma_{\mathcal{G}}(s, t_0) \right) - \left( \max_{s \in \mathcal{R}_1^+(\mathcal{X})} \gamma_{\mathcal{G}}(s, \hat{s}_m) + \gamma_{\mathcal{G}}(s, \hat{t}_m) \right) \right| \\ &\leq \left| \max_{s \in \mathcal{R}_1^+(\mathcal{X})} \gamma_{\mathcal{G}}(s, s_0) + \gamma_{\mathcal{G}}(s, t_0) - (\gamma_{\mathcal{G}}(s, \hat{s}_m) + \gamma_{\mathcal{G}}(s, \hat{t}_m)) \right| \\ &= \left| \max_{s \in \mathcal{R}_1^+(\mathcal{X})} (\gamma_{\mathcal{G}}(s, s_0) - \gamma_{\mathcal{G}}(s, \hat{s}_m) + \gamma_{\mathcal{G}}(s, t_0) - \gamma_{\mathcal{G}}(s, \hat{t}_m)) \right| \\ &\leq \left| (\gamma_{\mathcal{G}}(\hat{s}_m, s_0) + \gamma_{\mathcal{G}}(\hat{t}_m, t_0)) \right| \quad (\because \gamma_{\mathcal{G}} \text{ satisfies Triangle Inequality}) \end{aligned}$$

□

We now prove the Theorem 3.8 for  $q > 1$  case.

$$\bar{\mathcal{U}}_q^q(s_0, t_0) \equiv \min_{\pi \in \mathcal{R}^+(\mathcal{X} \times \mathcal{X})} h(\pi, s_0, t_0) \equiv \left( \int c^p \, d\pi \right)^{q/p} + \lambda \gamma_{\mathcal{G}}^q(\pi_1, s_0) + \lambda \gamma_{\mathcal{G}}^q(\pi_2, t_0)$$

Now, we have:

$$\begin{aligned} \bar{\mathcal{U}}_q^q(s_m, t_m) - \bar{\mathcal{U}}_q^q(s_0, t_0) &= \min_{\pi \in \mathcal{R}^+(\mathcal{X} \times \mathcal{X})} h(\pi, \hat{s}_m, \hat{t}_m) - \min_{\pi \in \mathcal{R}^+(\mathcal{X} \times \mathcal{X})} h(\pi, s_0, t_0) \\ &\leq h(\pi^*, \hat{s}_m, \hat{t}_m) - h(\pi^*, s_0, t_0) \quad \left( \text{where } \pi^* = \arg \min_{\pi \in \mathcal{R}^+(\mathcal{X} \times \mathcal{X})} h(\pi, s_0, t_0) \right) \\ &= \lambda (\gamma_{\mathcal{G}}^q(\pi_1^*, \hat{s}_m) - \gamma_{\mathcal{G}}^q(\pi_1^*, s_0) + \gamma_{\mathcal{G}}^q(\pi_2^*, \hat{t}_m) - \gamma_{\mathcal{G}}^q(\pi_2^*, t_0)) \\ &= \lambda \left( (\gamma_{\mathcal{G}}(\pi_1^*, \hat{s}_m) - \gamma_{\mathcal{G}}(\pi_1^*, s_0)) \left( \sum_{i=0}^{q-1} \gamma_{\mathcal{G}}^i(\pi_1^*, \hat{s}_m) \gamma_{\mathcal{G}}^{q-1-i}(\pi_1^*, s_0) \right) \right) + \\ &\quad \lambda \left( (\gamma_{\mathcal{G}}(\pi_2^*, \hat{t}_m) - \gamma_{\mathcal{G}}(\pi_2^*, t_0)) \left( \sum_{i=0}^{q-1} \gamma_{\mathcal{G}}^i(\pi_2^*, \hat{t}_m) \gamma_{\mathcal{G}}^{q-1-i}(\pi_2^*, t_0) \right) \right) \\ &\leq \lambda \left( \gamma_{\mathcal{G}}(s_0, \hat{s}_m) \left( \sum_{i=0}^{q-1} \gamma_{\mathcal{G}}^i(\pi_1^*, \hat{s}_m) \gamma_{\mathcal{G}}^{q-1-i}(\pi_1^*, s_0) \right) \right) + \\ &\quad \lambda \left( \gamma_{\mathcal{G}}(t_0, \hat{t}_m) \left( \sum_{i=0}^{q-1} \gamma_{\mathcal{G}}^i(\pi_2^*, \hat{t}_m) \gamma_{\mathcal{G}}^{q-1-i}(\pi_2^*, t_0) \right) \right) \quad (\because \gamma \text{ satisfies Triangle Inequality}) \\ &\leq \lambda \left( \gamma_{\mathcal{G}}(s_0, \hat{s}_m) \sum_{i=0}^{q-1} \left( \binom{q-1}{i} \gamma_{\mathcal{G}}^i(\pi_1^*, \hat{s}_m) \gamma_{\mathcal{G}}^{q-1-i}(\pi_1^*, s_0) \right) \right) + \\ &\quad \lambda \left( \gamma_{\mathcal{G}}(t_0, \hat{t}_m) \left( \sum_{i=0}^{q-1} \binom{q-1}{i} \gamma_{\mathcal{G}}^i(\pi_2^*, \hat{t}_m) \gamma_{\mathcal{G}}^{q-1-i}(\pi_2^*, t_0) \right) \right) \end{aligned}$$

$$\begin{aligned}
&= \lambda \left( \gamma_{\mathcal{G}}(s_0, \hat{s}_m) (\gamma_{\mathcal{G}}(\pi_1^*, \hat{s}_m) + \gamma_{\mathcal{G}}(\pi_1^*, s_0))^{q-1} + \gamma_{\mathcal{G}}(t_0, \hat{t}_m) (\gamma_{\mathcal{G}}(\pi_2^*, \hat{t}_m) + \gamma_{\mathcal{G}}(\pi_2^*, t_0))^{q-1} \right) \\
&\leq \lambda \left( \max(\bar{M}^{q-1}(\hat{s}_m, s_0), \bar{M}^{q-1}(\hat{t}_m, t_0)) (\gamma_{\mathcal{G}}(s_0, \hat{s}_m) + \gamma_{\mathcal{G}}(t_0, \hat{t}_m)) \right) \text{ (With } \bar{M} \text{ defined in E.2)}
\end{aligned}$$

For the last inequality, we use the following

$$\begin{aligned}
\gamma_{\mathcal{G}}(\pi_1^*, \hat{s}_m) + \gamma_{\mathcal{G}}(\pi_1^*, s_0) &\leq \max_{s \in \mathcal{R}_1^+(\mathcal{X})} \gamma_{\mathcal{G}}(s, \hat{s}_m) + \gamma_{\mathcal{G}}(s, s_0) \\
&= \bar{M}(\hat{s}_m, s_0)
\end{aligned}$$

Using Lemma E.2,  $\bar{M}(\hat{s}_m, s_0) \rightarrow \bar{M}(s_0, s_0)$  at the same rate as  $\gamma_{\mathcal{G}}(\hat{s}_m, s_0) \rightarrow 0$ .

The rate at which  $\bar{U}_q^q(s_m, t_m) - \bar{U}_q^q(s_0, t_0)$  goes to zero is hence same as that with which either of the IPM terms goes to zero. For example, if the IPM is MMD with a normalized kernel, then  $\gamma_{\mathcal{M}_k}(s_0, \hat{s}_m) \leq \sqrt{\frac{1}{m}} + \sqrt{\frac{2 \log(1/\delta)}{m}}$  with probability  $1 - \delta$  [60]. From the union bound, with probability  $1 - \delta$ ,  $\bar{U}_q^q(s_m, t_m) - \bar{U}_q^q(s_0, t_0) \leq 2\lambda \max(\bar{M}^{q-1}(s_0, s_0), \bar{M}^{q-1}(t_0, t_0)) \left( \sqrt{\frac{1}{m}} + \sqrt{\frac{2 \log(2/\delta)}{m}} \right)$ . Thus,  $O\left(\frac{1}{\sqrt{m}}\right)$  is the common bound for the rate at which the LHS as well as  $\gamma_{\mathcal{M}_k}(s_0, \hat{s}_m)$  decay to zero. In summary, the proposed metrics inherit their sample complexity from the IPM regularizers rather than from the Wasserstein metrics.

## E.2 Geodesics

The geometry of the space of measures depends on the distance with which the space is equipped with. In this section, we review some relevant facts from metric geometry and urge the interested readers to refer [9] for details.

Let  $\mathcal{X}$  be a Polish metric space endowed with a distance metric,  $d : \mathcal{X} \times \mathcal{X} \rightarrow \mathbb{R}^+ \cup \{\infty\}$  that defines its topology.

**Curve** The function  $\omega : t \in [a, b] \subset \mathbb{R} \mapsto \omega_t \in \mathcal{X}$  defines a curve connecting  $\omega_a$  and  $\omega_b$ . *Length* of the curve  $\omega$  connecting  $\omega_a$  and  $\omega_b$  is defined as

$$L(\omega, a, b) \equiv \sup_{n > 1} \sup_{a=t_0 < t_1 < \dots < t_n=b} \sum_{i=1}^n d(\omega_{t_{i-1}}, \omega_{t_i})$$

**Length Space** The metric space  $(\mathcal{X}, d)$  is a *length space* if

$$d(x, y) = \inf_{\omega: [a, b] \rightarrow \mathcal{X}; \text{ s.t. } \omega_a=x, \omega_b=y} L(\omega, a, b)$$

A curve  $\omega$  that achieves this infimum is the shortest path connecting  $\omega_a$  and  $\omega_b$  and is called the **Minimal Geodesic** connecting  $\omega_a$  and  $\omega_b$ . The distance  $d$  is called *strictly intrinsic* if  $d(x, y) < \infty$  for any two points  $x, y$  on the minimal geodesic curve.

**Characterizing Minimal Geodesics** We state the following theorem and corollary from [9] that characterize minimal geodesics.

**Theorem E.3.** (Restating Theorem 4.1 from [9]) Let  $\omega : [a, b] \rightarrow \mathcal{X}$  be a curve joining points  $\omega_a, \omega_b$  such that  $d(\omega_a, \omega_b) < \infty$ . This curve is a minimal geodesic of length  $d(\omega_a, \omega_b)$  iff  $\forall a \leq t \leq t' \leq b$ ,  $d(\omega_a, \omega_t) + d(\omega_t, \omega_{t'}) + d(\omega_{t'}, \omega_b) = d(\omega_a, \omega_b)$ .

**Corollary E.4.** (Restating Corollary 4.2 from [9]) Let  $\omega : [0, 1] \rightarrow \mathcal{X}$  be a curve joining  $\omega_0, \omega_1 \in \mathcal{X}$  such that  $d(\omega_0, \omega_1) < \infty$ . The following assertions are equivalent:

1. The curve  $\omega$  is a constant speed minimal geodesic of length  $d(\omega_0, \omega_1)$ .
2.  $\forall t, t' \in [0, 1]$ ,  $d(\omega_t, \omega_{t'}) = |t - t'| d(\omega_0, \omega_1)$ .

### E.2.1 Proof of Lemma 3.9

**Lemma E.5.** For any two measures  $s_0, s_1 \in \mathcal{R}^+(\mathcal{X})$ , the mixture measure  $\forall t \in [0, 1]$   $s_t = (1 - t)s_0 + ts_1$  form a curve in the space of distributions  $\mathcal{R}^+(\mathcal{X})$ . Any mixture curve joining two measures  $s_0, s_1 \in \mathcal{R}^+(\mathcal{X})$  such that  $\mathcal{U}_{\mathcal{G}, c, \lambda, 1, q}(s_0, s_1) < \infty$ , is a constant speed minimal geodesic, making  $\mathcal{U}_{\mathcal{G}, c, \lambda, 1, q}$  a strictly intrinsic distance.

*Proof.*

$$\begin{aligned}\mathcal{U}_{\mathcal{G},c,\lambda,1,q}(s_t, s'_t) &= \mathcal{U}_{\mathcal{G},c,\lambda,1,q}((1-t)s_0 + ts_1, (1-t')s_0 + t's_1) \\ &= \mathcal{U}_{\mathcal{G},c,\lambda,1,q}((t'-t)s_0, (t'-t)s_1) \\ &= |t-t'| \mathcal{U}_{\mathcal{G},c,\lambda,1,q}(s_0, s_1)\end{aligned}$$

The last two equalities use that  $\mathcal{U}_{\mathcal{G},c,\lambda,1,q}$  is a norm-induced metric (as proved in B and C). We then conclude the proof of Lemma 3.9 from the Corollary E.4.  $\square$

### E.3 Proof of Robustness Lemma 3.10

**Lemma E.6.** *Let  $s, t \in \mathcal{R}^+(\mathcal{X})$  be two measures such that  $s$  is corrupted with  $\rho$  fraction of outliers i.e.,  $s = (1-\rho)s_c + \rho s_o$ , where  $s_c$  is the clean measure and  $s_o$  is the outlier measure. Let  $|s_c - s_o|_{TV} \leq \epsilon$ . Let  $\beta = \max_{f \in \mathcal{G}(\lambda) \cap \mathcal{W}_c} \|f\|_\infty$ , then,*

$$\mathcal{U}_{\mathcal{G},c,\lambda,1,1}(s, t) \leq \mathcal{U}_{\mathcal{G},c,\lambda,1,1}(s_c, t) + \rho\beta\epsilon,$$

For the case  $q > 1$ ,

$$\mathcal{U}_{\mathcal{G},c,\lambda,1,q}(s, t) \leq \mathcal{U}_{\mathcal{G},c,\lambda,1,q}(s_c, t) + \frac{\eta^{1/q}}{\alpha^r} t \rho \beta \epsilon$$

where  $\frac{1}{q} + \frac{1}{r} = 1, t = \min\left(1, \frac{\lambda^{1/q}}{2^r}\right), \alpha = \frac{q-1}{q^r}, \eta = \frac{r-1}{r^q}$ .

*Proof.* We prove Lemma 3.10 for the case  $q = 1$  and  $q > 1$  separately.

**Case  $q = 1$ :**

We use the dual formulation of  $\mathcal{U}_{\mathcal{G},c,\lambda,1,1}$  which was proved in Theorem 3.4. We first upper-bound  $\mathcal{U}_{\mathcal{G},c,\lambda,1,1}(s_o, t)$  which we later use in proving the lemma.

$$\begin{aligned}\mathcal{U}_{\mathcal{G},c,\lambda,1,1}(s_o, t) &= \max_{f \in \mathcal{G}(\lambda) \cap \mathcal{W}_c} \int f ds_o - \int f dt \\ &= \max_{f \in \mathcal{G}(\lambda) \cap \mathcal{W}_c} \int f d(s_o - s_c) + \int f ds_c - \int f dt \\ &\leq \max_{f \in \mathcal{G}(\lambda) \cap \mathcal{W}_c} \int f d(s_o - s_c) + \max_{f \in \mathcal{G}(\lambda) \cap \mathcal{W}_c} \left( \int f ds_c - \int f dt \right) \\ &\leq \beta |s_c - s_o|_{TV} + \mathcal{U}_{\mathcal{G},c,\lambda,1,1}(s_c, t) \\ &= \beta \epsilon + \mathcal{U}_{\mathcal{G},c,\lambda,1,1}(s_c, t)\end{aligned} \tag{16}$$

$$\begin{aligned}\mathcal{U}_{\mathcal{G},c,\lambda,1,1}(s, t) &= \max_{f \in \mathcal{G}(\lambda) \cap \mathcal{W}_c} \int f ds - \int f dt \\ &= \max_{f \in \mathcal{G}(\lambda) \cap \mathcal{W}_c} (1-\rho) \int f ds_c + \rho \int f ds_o - \int f dt \\ &= \max_{f \in \mathcal{G}(\lambda) \cap \mathcal{W}_c} (1-\rho) \left( \int f ds_c - \int f dt \right) + \rho \left( \int f ds_o - \int f dt \right) \\ &\leq \max_{f \in \mathcal{G}(\lambda) \cap \mathcal{W}_c} (1-\rho) \left( \int f ds_c - \int f dt \right) + \max_{f \in \mathcal{G}(\lambda) \cap \mathcal{W}_c} \rho \left( \int f ds_o - \int f dt \right) \\ &= (1-\rho) \mathcal{U}_{\mathcal{G},c,\lambda,1,1}(s_c, t) + \rho \mathcal{U}_{\mathcal{G},c,\lambda,1,1}(s_o, t) \\ &\leq (1-\rho) \mathcal{U}_{\mathcal{G},c,\lambda,1,1}(s_c, t) + \rho (\mathcal{U}_{\mathcal{G},c,\lambda,1,1}(s_c, t) + \beta \epsilon) \quad (\text{Using 16}) \\ &= \mathcal{U}_{\mathcal{G},c,\lambda,1,1}(s_c, t) + \rho \beta \epsilon\end{aligned}$$

$\square$

**Case  $q > 1$ :** For this case, we use the joint convexity of  $\mathcal{U}_{\mathcal{G},c,\lambda,1,q}$  proved in the following lemma.

**Lemma E.7.**  $\mathcal{U}_{\mathcal{G},c,\lambda,1,q}$  is jointly convex.

*Proof.* The  $q^{th}$  root of the objective in (6) can be written as  $h(x) \equiv \|(h_1(x), h_2(x), h_3(x))\|_q$ , where  $x \equiv (s, t, s_0, t_0)$ . Now, each  $h_i$  is pointwise maximum of linear functions in  $x$  as each is either  $W_1$  or  $\gamma_G$ . Domains of  $h_i$  are also convex. Hence each  $h_i$  is convex. By convexity preserving vector composition rules (for e.g., Section 3.2.4 in [10], we have that  $h(x)$  is also convex. Indeed,  $h_i \geq 0$  are convex and  $\|\cdot\|_q$  is convex and non-increasing in each entry over non-negative orthant. Now, since  $\mathcal{U}(s_0, t_0) = \min_{s,t} h(s, t, s_0, t_0)$ , where  $h$  is convex, we have that  $\mathcal{U}$  is also convex (see for e.g., Section 3.2.5 in [10]).  $\square$

We now prove Lemma 3.10 for the case  $q > 1$ .

*Proof.*

$$\begin{aligned}
\mathcal{U}_{\mathcal{G},c,\lambda,1,q}((1-\rho)s_c + \rho s_o, t) - \mathcal{U}_{\mathcal{G},c,\lambda,1,q}(s_c, t) &\leq (1-\rho)\mathcal{U}_{\mathcal{G},c,\lambda,1,q}(s_c, t) + \rho\mathcal{U}_{\mathcal{G},c,\lambda,1,q}(s_o, t) \\
&\quad - \mathcal{U}_{\mathcal{G},c,\lambda,1,q}(s_c, t) \quad (\text{Using Lemma E.7}) \\
&= \rho(\mathcal{U}_{\mathcal{G},c,\lambda,1,q}(s_o, t) - \mathcal{U}_{\mathcal{G},c,\lambda,1,q}(s_c, t)) \\
&\leq \rho\mathcal{U}_{\mathcal{G},c,\lambda,1,q}(s_c, s_o) \quad (\text{From Triangle Inequality}) \\
&= \rho \left( \min_{\mu, \nu \in \mathcal{F}; \mu+\nu=s_o-s_c} \frac{\eta}{\alpha^{q-1}} \|\mu\|_W^q + \frac{\eta\lambda}{(2\alpha)^{q-1}} \|\nu\|^q \right)^{\frac{1}{q}} \\
&\leq \rho \left( \min_{\mu \in \mathcal{F}, \nu=0; \mu+\nu=s_o-s_c} \frac{\eta}{\alpha^{q-1}} \|\mu\|_W^q + \frac{\eta\lambda}{(2\alpha)^{q-1}} \|\nu\|^q \right)^{\frac{1}{q}} \\
&\leq \frac{\eta^{1/q}}{\alpha^r} \rho\beta |s_o - s_c|_{TV} \tag{17} \\
&\leq \frac{\eta^{1/q}}{\alpha^r} \rho\beta\epsilon \tag{18}
\end{aligned}$$

Similarly,

$$\begin{aligned}
\mathcal{U}_{\mathcal{G},c,\lambda,1,q}((1-\rho)s_c + \rho s_o, t) - \mathcal{U}_{\mathcal{G},c,\lambda,1,q}(s_c, t) &\leq \rho \left( \min_{\mu=0, \nu \in \mathcal{F}; \mu+\nu=s_o-s_c} \frac{\eta}{\alpha^{q-1}} \|\mu\|_W^q + \frac{\eta\lambda}{(2\alpha)^{q-1}} \|\nu\|^q \right)^{\frac{1}{q}} \\
&\leq \frac{\eta^{1/q}}{\alpha^r} \frac{\lambda^{\frac{1}{q}}}{2^r} \rho\beta |s_o - s_c|_{TV} \tag{19} \\
&\leq \frac{\eta^{1/q}}{\alpha^r} \frac{\lambda^{\frac{1}{q}}}{2^r} \rho\beta\epsilon \tag{20}
\end{aligned}$$

From 18 and 20,

$$\mathcal{U}_{\mathcal{G},c,\lambda,1,q}((1-\rho)s_c + \rho s_o, t) - \mathcal{U}_{\mathcal{G},c,\lambda,1,q}(s_c, t) \leq \frac{\eta^{\frac{1}{q}}}{\alpha^r} \min \left( 1, \frac{\lambda^{\frac{1}{q}}}{2^r} \right) \rho\beta\epsilon$$

$\square$

## F Proof of Lemma 3.11

*Proof.* Let  $f(\alpha)$  denote the objective of the proposed formulation 9. We denote  $G_1, G_2$  as the Gram matrices over the source and target samples respectively and  $m_1, m_2$  as the number of source and target samples respectively.

$$\nabla f(\alpha) = \mathcal{C}_{12} + 2(\lambda_1 G_1 \alpha \mathbf{1}_{m_2} \mathbf{1}_{m_2}^\top + \lambda_2 \mathbf{1}_{m_1} \mathbf{1}_{m_1}^\top \alpha G_2)$$

We now derive the Lipschitz-constant of this gradient. Without loss of generality, we derive for the case  $\lambda_1 = \lambda_2 = \lambda$ .

$$\begin{aligned}
\nabla f(\alpha) - \nabla f(\beta) &= 2\lambda (G_1 (\alpha - \beta) \mathbf{1}_{m_2} \mathbf{1}_{m_2}^\top + \mathbf{1}_{m_1} \mathbf{1}_{m_1}^\top (\alpha - \beta) G_2) \\
\text{vec}(\nabla f(\alpha) - \nabla f(\beta)) &= 2\lambda (\text{vec}(G_1 (\alpha - \beta) \mathbf{1}_{m_2} \mathbf{1}_{m_2}^\top) + \text{vec}(\mathbf{1}_{m_1} \mathbf{1}_{m_1}^\top (\alpha - \beta) G_2)) \\
&= 2\lambda (\mathbf{1}_{m_2} \mathbf{1}_{m_2}^\top \otimes G_1 + G_2 \otimes \mathbf{1}_{m_1} \mathbf{1}_{m_1}^\top) \text{vec}(\alpha - \beta)
\end{aligned}$$

Thus,  $\|\text{vec}(\nabla f(\alpha) - \nabla f(\beta))\|_F \leq 2\lambda \|\mathbf{1}_{m_2} \mathbf{1}_{m_2}^\top \otimes G_1 + G_2 \otimes \mathbf{1}_{m_1} \mathbf{1}_{m_1}^\top\|_F \|\text{vec}(\alpha - \beta)\|_F$  (from Cauchy Schwarz). This implies, the Lipschitz smoothness constant  $L = 2\lambda \|\mathbf{1}_{m_2} \mathbf{1}_{m_2}^\top \otimes G_1 + G_2 \otimes \mathbf{1}_{m_1} \mathbf{1}_{m_1}^\top\|_F = 2\lambda \sqrt{m_2^2 \|G_1\|^2 + m_1^2 \|G_2\|^2 + 2(\mathbf{1}_{m_1}^\top G_1 \mathbf{1}_{m_1} + \mathbf{1}_{m_2}^\top G_2 \mathbf{1}_{m_2})}$   $\square$

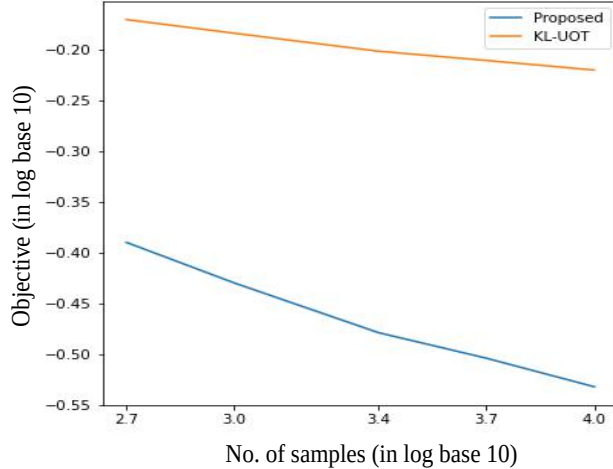


Figure 3: The objective values of KL-UOT and the proposed formulation is shown as the number of samples increase. The data lies in 500 dimensions and the source and target marginals are both Uniform. The proposed formulation can be seen to have a better rate of convergence.

## G Experiments

We present more experimental details and additional results in this section. We will open-source the codes to reproduce all our experiments upon acceptance of the paper.

### G.1 Synthetic Experiments

**Sample Complexity** In Section E.1, we proved dimension-free sample complexity of the proposed metrics. In this section, we present a synthetic experiment to show that the convergence of the proposed objective is faster than KL-UOT’s objective. We sample 100-dimensional source and target samples from Uniform source and target marginals respectively. As the marginals are equal, the metrics over measures should converge to 0 as the number of samples increase. We repeat the experiment with increasing number of samples. In our experimental setup, we follow conditions given in [37] so that KL-UOT becomes a square of metric. We used squared-Euclidean cost for KL-UOT,  $\lambda = 1$  and no entropic regularization (for metricity). For the proposed formulation, Euclidean cost was used with squared-MMD regularization, RBF kernel and  $\sigma$  as 1. We show the proposed objective and the square-root of the KL-UOT objective on increasing the number of samples in Figure 3. It can be seen from the plot that the proposed formulation achieves a better rate of convergence compared to KL-UOT.

**Effect of Regularization** We experiment on synthetic data with a bimodal distribution and observe the effect of regularization on the transport plans of the proposed method. Figure 4 shows marginals of transport plans with normalized measures (balanced case) and un-normalized measures (unbalanced case) respectively. The source and target measures are shown using dashed lines and plans are the filled plots. On increasing regularization, the match between marginals of the transport plan and the given source and target marginals become better. Euclidean distance is used as the ground cost metric and the regularization is squared-MMD. IMQ kernel with hyperparameter  $K^2$  as  $10^{-6}$  is used in all our results.

**Barycenter with Gaussian measures** We experiment with source and target measures as Gaussian and compare our barycenters with those obtained with MMD and  $\epsilon$ KL-UOT. The rows in 5 are for the case with normalized and un-normalized Gaussian measures respectively. Interpolation by MMD is the empirical average of two measures and is denoted by Avg. Sinkhorn-stabilized barycenter solver from the Python-OT (POT) library are used for OT and  $\epsilon$ KL-UOT.

**Level Sets with the Proposed Metric** Level sets of 2-Wasserstein (OT with no regularization) with squared-Euclidean ground metric are shown. For MMD, RBF kernel is used with  $\sigma^2$  as 3. Level sets of GW-TV have Euclidean distance as the ground metric and  $\lambda$  as 10. For the proposed method, the chosen hyper-parameters are: squared-Euclidean cost as the ground metric,  $\lambda$  as 10, squared-MMD regularization and RBF kernel with  $\sigma^2$  as 2. Sigma values for kernels are

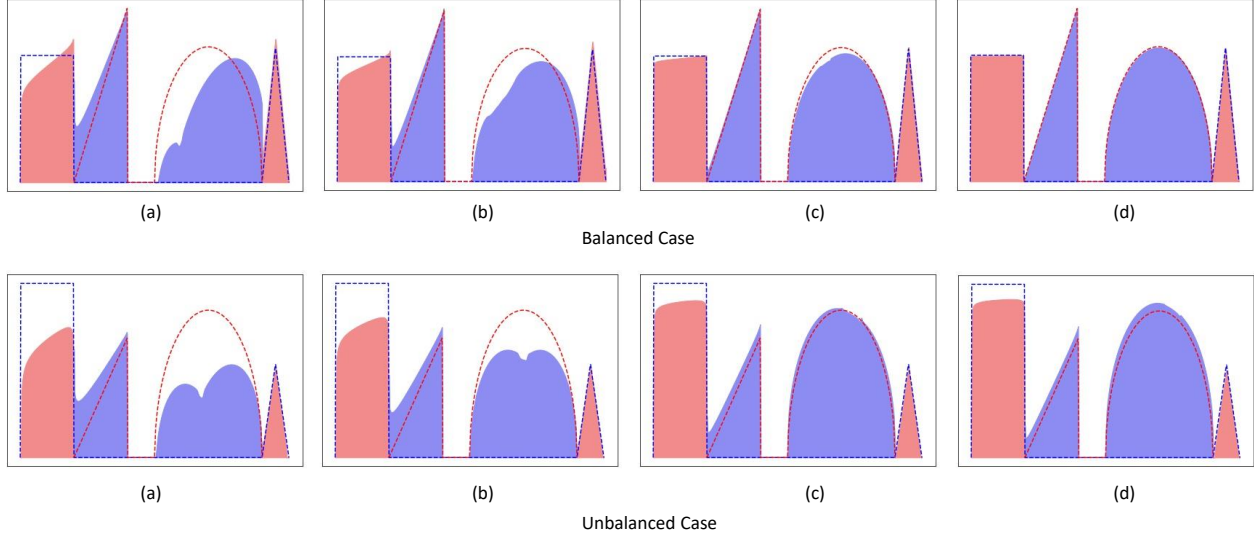


Figure 4: Effect of increasing regularization in Synthetic Bimodal example

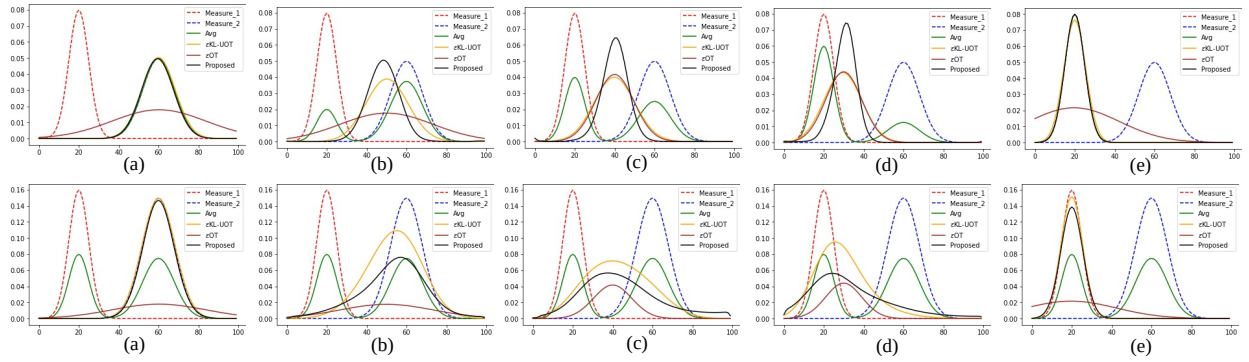


Figure 5: Barycenter with Gaussian Measures. The first row is with normalized measures and the second row is with un-normalized measures.

chosen based on the median heuristics and lambda values are chosen based on the scale of terms in the objective. For plotting contour plots, the hyperparameter specifying total number of lines is 20 for all methods.

**Transport plan in outlier-setting** For all the methods, Euclidean distance metric is taken as ground cost. The regularization coefficient chosen for GW-TV, ROT, RSOT are 0.4, 0.1 and 0.1 respectively. For the proposed method,  $\lambda$  is chosen as 0.1, MMD regularization is employed with RBF kernel and  $\sigma^2$  as  $10^{-3}$ .

## G.2 Single cell RNA sequencing

Embryoid Body dataset comprises of data at 5 timesteps with sample sizes as 2381, 4163, 3278, 3665 and 3332 respectively. For the task of prediction at timestep  $t_i$ , the data was standardized using statistics of data from  $\{t_0, t_1, t_2, t_3, t_4\} \setminus \{t_i\}$ . For the proposed method, constant  $K^2$ , of the IMQ kernel is chosen from  $\{1e-3, 1e-4, 1e-5\}$  and  $\lambda$  is chosen from  $\{1, 1e-1, 1e-2\}$ . For  $\epsilon$ KL-UOT,  $\lambda$  is chosen from  $\{1, 1e-1, 1e-2\}$  and the coefficient of entropic regularization is chosen from  $\{1e-1, 1e-3, 1e-5\}$ . For  $\epsilon$ KL-UOT, the chosen hyper-parameters  $(\lambda, \epsilon)$  where  $\lambda$  is the coefficient of KL regularization and  $\epsilon$  is the coefficient of entropic regularization are:  $(1, 10^{-5})$ ,  $(1, 10^{-3})$ ,  $(10^{-2}, 10^{-1})$  at timesteps  $t_1, t_2, t_3$  respectively. For the proposed method, the coefficient of squared-MMD regularization ( $\lambda$ ) is chosen as 0.1 and the constant  $K^2$  used in the IMQ kernel is chosen as  $10^{-3}$  at all timesteps.

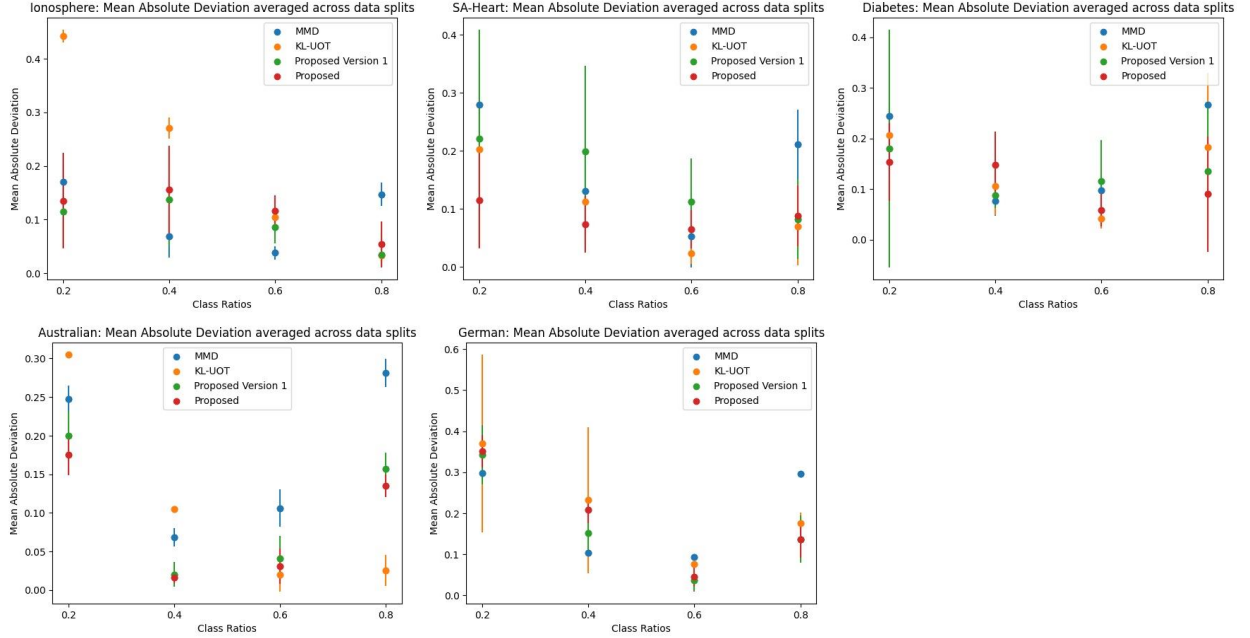


Figure 6: Mean Absolute Deviation averaged across data splits shown separately for each class ratio

Table 6: Mean Absolute Deviation (lesser is better) averaged across data splits

DATASET	MMD	$\epsilon$ KL-UOT	PROPOSED VERSION 1	PROPOSED
IONOSPHERE	0.106 $\pm$ 0.027	0.212 $\pm$ 0.013	<b>0.093<math>\pm</math>0.050</b>	0.116 $\pm$ 0.061
SAHEART	0.169 $\pm$ 0.059	0.102 $\pm$ 0.042	0.154 $\pm$ 0.120	<b>0.085 <math>\pm</math>0.054</b>
DIABETES	0.171 $\pm$ 0.029	0.134 $\pm$ 0.069	0.129 $\pm$ 0.119	<b>0.112<math>\pm</math>0.072</b>
AUSTRALIAN	0.175 $\pm$ 0.018	0.114 $\pm$ 0.011	0.105 $\pm$ 0.025	<b>0.089<math>\pm</math>0.018</b>
GERMAN	0.198 $\pm$ 0.008	0.214 $\pm$ 0.106	<b>0.167<math>\pm</math>0.053</b>	0.185 $\pm$ 0.035

### G.3 Domain Adaptation in JUMBOT framework

The accuracies shown in Table 3 are averages across three independent trials with the same seed as used by JUMBOT. For Digits dataset, we use MMD regularization along with an L2-regularization on the transport matrix with coefficient 100. The chosen hyper-parameters for Digits experiment are IMQ kernel with constant  $K^2$  as 1,  $\lambda$  as 10 and MMD regularization. For VisDA experiment, the chosen hyper-parameters are RBF kernel with constant  $\sigma^2$  as 60,  $\lambda$  as 10 and squared-MMD regularization.

### G.4 Class Ratio Experiment

We experiment on Five UCI datasets- Australian, Ionosphere, SA-Heart, Diabetes and German Credit data. Based on an initial random seed, we divide the data into a training set and a test set. The (training set size, test set size) for Australian, Ionosphere, SA-Heart, Diabetes and German datasets are (454, 100), (172, 50), (192, 80), (376, 100) and (400, 100) respectively. Hyperparameters are tuned on 30 validation sets that are randomly sampled from the training set. The ratio of classes in the training sets is 0.5. We report the results on the test set with the best hyperparameter after repeating the experiment with 4 initial random seeds.

In the main paper, we presented results with the proposed formulation where we take union of source and target data as the support of the transport matrix. Here, we also present results with the proposed method where the transport matrix is parameterized by source and target samples on the two sides respectively, i.e.  $\alpha \in \mathbb{R}^{m_1 \times m_2}$ . We refer to it as **proposed version 1**. Table 6 shows that proposed version 1 also performs better than both MMD and  $\epsilon$ KL-UOT baselines on Four out of the Five datasets. In Figure 6, we present the Mean Absolute Deviations averaged across data splits for each class ratio separately.



Table 7: Hyperparameters for class ratio experiment with Ionosphere dataset

CLASS-RATIO	MMD $\sigma$	$\epsilon$ KL-UOT ( $\lambda, \epsilon$ )	PROPOSED VERSION 1 ( $\lambda, \sigma$ )	PROPOSED ( $\lambda, \sigma$ )
0.2	0.1	$(10^{-2}, 10^{-1})$	(10, 1)	(0.1, 10)
0.4	0.1	$(10^{-2}, 10^{-1})$	(10, 1)	(0.1, 10)
0.6	0.1	$(10^{-2}, 10^{-1})$	(10, 1)	(0.1, 1)
0.8	0.1	$(1, 10^{-1})$	(10, 1)	(1, 1)

Table 8: Hyperparameters for class ratio experiment with Diabetes dataset

CLASS-RATIO	MMD $\sigma$	$\epsilon$ KL-UOT ( $\lambda, \epsilon$ )	PROPOSED VERSION 1 ( $\lambda, \sigma$ )	PROPOSED ( $\lambda, \sigma$ )
0.2	50	$(10^{-1}, 10^{-3})$	(10, 200)	(1, 200)
0.4	50	$(10^{-1}, 10^{-3})$	(1, 100)	(1, 100)
0.6	50	$(10^{-2}, 10^{-2})$	(1, 150)	(1, 200)
0.8	50	$(10^{-1}, 10^{-3})$	(1, 200)	(1, 200)

For proposed version 1 and proposed formulation,  $\lambda$  is chosen from  $\{0.1, 1, 10\}$  for Ionosphere dataset, from  $\{0.01, 0.1, 1\}$  for Australian and German datasets, from  $\{1, 10, 100\}$  for Diabetes dataset and from  $\{0.1, 1, 10\}$  for SAHeart dataset. The constant hyperparameter used in IMQ kernel is chosen from  $\{1, 10, 20\}$  for Ionosphere and from  $\{100, 150, 200\}$  for all other datasets. The pool of hyperparameters is chosen based on scale of terms in the involved objective functions and the condition numbers of Gram matrices.

For MMD, RBF kernel is used as it resulted in better optimization compared to IMQ kernel. For validation, the pool of  $\sigma^2$  values was  $\{10, 20, 30\}$  for Australian and German datasets,  $\{0.01, 0.05, 0.1\}$  for Ionosphere,  $\{30, 40, 50\}$  for SA-Heart and  $\{30, 40, 50\}$  for Diabetes dataset. The chosen  $\sigma^2$  values are 20 for Australian, 0.1 for Ionosphere, 50 for SA-Heart and 50 for Diabetes dataset. For German dataset,  $\sigma^2$  was chosen as 30 for class ratio's 0.2 and 0.4 and it was chosen as 20 for class ratio's 0.6 and 0.8.

For  $\epsilon$ KL-UOT,  $\lambda$  is chosen from  $\{0.1, 0.01, 0.001\}$  for Australian dataset and from  $\{1, 0.1, 0.01\}$  for all other datasets. The entropic regularizer,  $\epsilon$ , is chosen from  $\{0.1, 0.01, 0.001\}$ . The pool of hyperparameters is chosen based on the scale of terms in the objective. We note that for the  $\epsilon$ KL-UOT optimization, optimal  $\theta$  at iteration  $k$  is  $\theta_k = [\sum_{i:y_i=0} \alpha_k^\top \mathbf{1}_i, \sum_{i:y_i=1} \alpha_k^\top \mathbf{1}_i]$ . The hyper-parameters chosen after validation are listed in Tables 7, 8, 9, 10 and 11.

#### G.4.1 Classification Accuracy

For OT based methods, we further use the transport matrix for getting classification accuracy on test data. To this end, we first compute the Barycentric projection of test data onto source data and label a test point based on the source point nearest to its Barycentric projection. For a sample  $x$ , the Barycentric projection of sample  $x$  is  $T(x) \equiv \operatorname{argmin}_{y \in \mathcal{Y}} \mathbb{E}[c(y, Y)|x]$ . In our experiment, cost  $c$  is squared-Euclidean.

We note that this classification experiment was performed using the same set of hyperparameters that were chosen after validating for Mean Absolute Deviation. The results are shown in Table 12 where we outperform the baselines.

Table 9: Hyperparameters for class ratio experiment with Australian dataset

CLASS-RATIO	MMD $\sigma$	$\epsilon$ KL-UOT ( $\lambda, \epsilon$ )	PROPOSED VERSION 1 ( $\lambda, \sigma$ )	PROPOSED ( $\lambda, \sigma$ )
0.2	20	$(10^{-3}, 10^{-1})$	(1, 200)	(1, 200)
0.4	20	$(10^{-3}, 10^{-1})$	(1, 200)	(1, 200)
0.6	20	$(10^{-2}, 10^{-3})$	(0.01, 150)	(0.1, 150)
0.8	20	$(10^{-1}, 10^{-3})$	(0.01, 200)	(0.01, 200)

Table 10: Hyperparameters for class ratio experiment with German dataset

CLASS-RATIO	MMD $\sigma$	$\epsilon$ KL-UOT ( $\lambda, \epsilon$ )	PROPOSED VERSION 1 ( $\lambda, \sigma$ )	PROPOSED ( $\lambda, \sigma$ )
0.2	30	$(1, 10^{-3})$	(1, 100)	(1, 100)
0.4	30	$(10^{-1}, 10^{-3})$	(1, 100)	(0.1, 100)
0.6	20	$(10^{-2}, 10^{-1})$	(0.1, 100)	(1, 200)
0.8	20	$(10^{-2}, 10^{-3})$	(0.01, 200)	(0.01, 200)

Table 11: Hyperparameters for class ratio experiment with SA-Heart dataset

CLASS-RATIO	MMD $\sigma$	$\epsilon$ KL-UOT ( $\lambda, \epsilon$ )	PROPOSED VERSION 1 ( $\lambda, \sigma$ )	PROPOSED ( $\lambda, \sigma$ )
0.2	50	$(1, 10^{-3})$	(10, 100)	(1, 200)
0.4	50	$(10^{-2}, 10^{-1})$	(10, 100)	(1, 100)
0.6	50	$(10^{-2}, 10^{-2})$	(10, 150)	(0.1, 200)
0.8	50	$(10^{-2}, 10^{-3})$	(1, 100)	(10, 200)

### G.5 Two-sample Test

Following [38], we repeat the experiment 10 times and in each trial, we randomly sample a validation subset and a test subset of size  $N$  from the given real and fake MNIST datasets. We run the two-sample test experiment for type-I error and type-II error on the test set for a given trial using the hyperparameters chosen for that trial. The hyperparameters were tuned for  $N = 100$  for each trial. The hyperparameters for a given trial were chosen based on the average empirical test-power (higher is better) over that trial’s validation dataset.

We use squared-Euclidean distance for the proposed and KL-UOT formulations. RBF kernel was used for MMD and for the squared-MMD regularized proposed formulation. The hyperparameters are chosen from the following set. For the proposed and MMD,  $\sigma$  was chosen from {median, 40, 60, 80, 100} where median is the median of Euclidean distances between the samples. For the proposed method,  $\lambda$  was chosen from {0.1, 1, 10, 100}. For  $\epsilon$ -KL-UOT,  $\lambda$  was chosen from {1,  $10^{-1}$ ,  $10^{-2}$ ,  $10^{-3}$ } and  $\epsilon$  was chosen from {1,  $10^{-1}$ ,  $10^{-2}$ ,  $10^{-3}$ ,  $10^{-4}$ }. The best hyperparameters found after validation are listed in Table 13.

### G.6 Computation Time

We present the Objective vs Time plot in Figure 7 where the proposed formulation is solved using accelerated projected gradient descent with the Lipschitz constant derived in Lemma F. The source and target measures are Uniform distributions from which we sample 100 data points each. The dimensionality of data is 100. The experiment was done with hyper-parameters as squared-Euclidean distance, squared-MMD regularization with RBF kernel and sigma as 1 and lambda as 0.1. We use the convergence criteria mentioned in [59]. This experiment was done on an NVIDIA-DGX GPU.

Table 12: Mean Accuracy (in %) after Domain Adaptation (higher is better) averaged across data splits

DATASET	$\epsilon$ KL-UOT	PROPOSED VERSION 1	PROPOSED
IONOSPHERE	51.1 $\pm$ 0.063	<b>82.1<math>\pm</math>0.041</b>	80.3 $\pm$ 0.038
SAHEART	57.2 $\pm$ 0.038	<b>57.9<math>\pm</math>0.071</b>	57.8 $\pm$ 0.040
DIABETES	59.3 $\pm$ 0.049	<b>64.5 <math>\pm</math>0.050</b>	63.9 $\pm$ 0.033
AUSTRALIAN	44.2 $\pm$ 0.141	<b>45.2<math>\pm</math>0.125</b>	44.8 $\pm$ 0.124
GERMAN	50.8 $\pm$ 0.046	<b>51.3<math>\pm</math>0.059</b>	51.1 $\pm$ 0.052

Table 13: Hyperparameters for Two-Sample test experiment on MNIST

TRIAL	MMD $\sigma$	$\epsilon$ KL-UOT ( $\lambda, \epsilon$ )	PROPOSED ( $\lambda, \sigma$ )
1	MEDIAN	$(10^{-2}, 10^{-1})$	(1, 100)
2	MEDIAN	$(1, 10^{-1})$	(0.1, 100)
3	MEDIAN	$(1, 10^{-3})$	(100, 100)
4	MEDIAN	$(1, 10^{-1})$	(1, MEDIAN)
5	MEDIAN	$(10^{-3}, 10^{-2})$	(1, MEDIAN)
6	MEDIAN	$(1, 10^{-1})$	(1, MEDIAN)
7	MEDIAN	$(1, 10^{-1})$	(1, MEDIAN)
8	80	$(1, 10^{-1})$	(1, MEDIAN)
9	MEDIAN	$(1, 10^{-1})$	(1, MEDIAN)
10	MEDIAN	$(1, 10^{-1})$	$(10^{-1}, 10)$

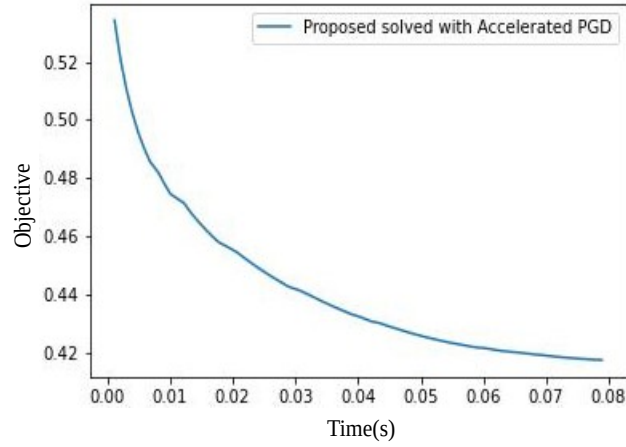


Figure 7: The objective of the proposed formulation (until convergence) vs time(s) with number of samples as 100.